UNIVERSIDADE DA BEIRA INTERIOR

UBI
Covilhã
Portugal

Design of a Variable-Span Morphing Wing

Elaborado por

João Rafael da Conceição Mestrinho

Orientado por

Dr. Pedro Gamboa

Dissertação submetida à Universidade da Beira Interior
para obtenção do grau de Mestre

na

Faculdade de Engenharia
Departamento de Ciências Aeroespaciais

Julho 2009

UNIVERSITY OF BEIRA INTERIOR

Abstract

Faculty of Engineering
Aerospacial Sciences Department

Master Thesis

by João Rafael da Conceição Mestrinho

The present work focuses on the study, design and validation of a variable-span morphing wing to be fitted to the UAV "Olharapo". Using an optimization code, which uses a viscous two-dimensional panel method formulation coupled with a non-linear liftingline algorithm and a sequential quadratic programming optimization routine, an aerodynamic analysis is performed to estimate the optimal values of wing span which ensure minimum drag across the flight speed envelope. The UAV flies in a relatively short speed range - from about 12 m/s to 30 m/s. Near its maximum speed it is possible to obtain a 20% drag reduction with the variable-span wing in comparison with the original fixed wing. A stability analysis is also performed to estimate the roll rate available with asymmetric span control. The variable-span wing matches the aileron in terms of roll power and maximum roll rate. It is concluded that roll control is possible with asymmetric span control. A new electro-mechanical actuation mechanism is developed using a simple and cheap rack and pinion system. The wing model is designed with graphical CAD/CAM tools and then a full scale model is built for bench testing the wing/actuator system. The concepts used on the morphing wing for both fixed and movable part are considered simple and effective. The actuation concept is also feasible but needs improvements in the attenuator. A powerful servo is also needed to more easily deploy the wing. Some future modifications at structural level and ideas for an in-flight automatic span controller are also presented.

Keywords: Aircraft Design; Morphing; Span Change; Telescopic Wing; UAV.

UNIVERSIDADE DA BEIRA INTERIOR

Resumo

Faculdade de Engenharia
Departamento de Ciências Aeroespaciais

Tese de Mestrado

por João Rafael da Conceição Mestrinho

O presente trabalho centra-se no estudo, concepção e validação de uma asa de envergadura variável para aplicação no UAV "Olharapo". Usando um código de optimização, que usa uma formulação de painéis viscoso bidimensional acoplado a um algoritmo de linha sustentadora não-linear e uma rotina de optimização de programação sequencial quadrática, é realizada uma análise aerodinâmica para estimar os valores óptimos de envergadura de forma a garantir um arrasto mínimo para todas as velocidades do envelope de voo. O UAV opera numa gama de velocidades relativamente pequena - de 12 m/s a 30 m/s, sensivelmente. Próximo da velocidade máxima é possível obter uma redução de 20% no arrasto com a asa de envergadura variável em comparação com a asa fixa original. É realizada uma análise de estabilidade com o objectivo de estimar a taxa de rolamento disponível com controlo assimétrico de envergadura. O desempenho da asa de envergadura variável é idêntico ao da asa original com ailerons em termos de poder de rolamento e de taxa de rolamento. Conclui-se que o controlo de rolamento pode ser efectuado com controlo assimétrico da envergadura. É feita a concepção de um novo sistema actuador electro-mecânico recorrendo a um sistema simples de pinhão e cremalheira. O modelo da asa é projectado recorrendo a ferramentas CAD/CAM e posteriormente construído para que o sistema asa/actuador seja testado em bancada. Os conceitos usados na asa *morphing* para a parte fixa e móvel são considerados simples e efectivos. O sistema de actuação é funcional mas necessita de melhoramentos ao nível do atenuador e requer um servo mais potente para uma actuação da asa mais fácil. Algumas modificações futuras a nível estrutural e algumas ideias para o desenvolvimento de um controlador para regulação automática da envergadura são também apresentadas.

Palavras-chave: Projecto de Aeronaves; *Morphing*; Variação de Envergadura; Asa Telescópica; UAV.

Acknowledgements

I would like to thank Dr. Pedro Gamboa for his imense patience and diligence. Without his guidance this project would not have been possible.

I want to thank my family for their love and support through out the years.

I would like to give a special kiss to Tânia for her love and understanding, specially on those moments when I could not think about anything else but work.

I would like to give a big hug to my brother Miguel. I wish you all that is good in life.

Finally, I want to give a big kiss to my parents for their endless love and support, I owe them everything.

Contents

Abstract i

Resumo ii

Acknowledgements iii

List of Figures vi

List of Tables ix

Nomenclature x

1 Introduction 1
- 1.1 Motivation . . . 2
- 1.2 State of the Art . . . 3
  - 1.2.1 Telescopic Spars . . . 3
  - 1.2.2 Inflatable Wings . . . 6
  - 1.2.3 Stability Analysis . . . 10
  - 1.2.4 Aerodynamic and Aeroelastic Analysis . . . 12
  - 1.2.5 Fully Adaptive Model . . . 14
- 1.3 Objectives . . . 15
- 1.4 Dissertation Layout . . . 16

2 Aerodynamic Analysis 18
- 2.1 Aircraft Characteristics . . . 18
  - 2.1.1 Performance Requirements . . . 19
- 2.2 Aerodynamic Optimization . . . 19
  - 2.2.1 Shape Optimization Tool . . . 19
  - 2.2.2 Input Data Requirements . . . 20
- 2.3 Optimization Results . . . 23

3 Rolling Rate Analysis 27
- 3.1 Stability Concepts . . . 27
- 3.2 Mathematical Model . . . 29
- 3.3 Roll Rate Results . . . 33

4 System Design and Construction **38**
4.1 Wing Design 38
4.1.1 Outer Moving Wing 38
4.1.2 Inner Fixed Wing 41
4.2 Actuation Mechanism 43
4.2.1 Actuator Requirements 43
4.2.2 Sizing and Assembling 45
4.2.3 Actuator Bay 46

5 Wing Testing **48**
5.1 Final Assembly 48
5.2 Bench Testing 50

6 Summary **52**
6.1 Conclusions 52
6.2 Future Work 53

Bibliography **55**

List of Figures

1.1 Spider plot comparing performance of the base-design Firebee, the morphing airfoil Firebee and the morphing planform Firebee.[1] 3

1.2 Pneumatic spars and root rib.[3] 4

1.3 Inflatable wing cross-sections.[8] 7

1.4 SMA wires integrated on inflatable wing.[10] 8

1.5 Roll moment due to asymmetric span control.[17] 13

1.6 Extended wing section showing the three bar segment.[19] 15

2.1 UAV Olharapo. 19

2.2 Flow chart illustrating wing aerodynamic shape optimization design tool process.[5] 21

2.3 Comparison between airfoil SG 6042 original and modified. 22

2.4 Schematic illustration of the variable-span wing. 22

2.5 AOA variation with flight speed for both original and VSW. 23

2.6 Drag comparison between original and VSW. 25

2.7 VSW span variation. 25

2.8 Lift-to-drag ratio comparison for both wings. 26

2.9 Required power variation with flight speed. 26

3.1 AOA changes due to angular velocity p.[20] 28

3.2 Spanwise lift distribution due to rolling.[20] 29

3.3 Change in neutral roll point due to asymmetric variations in span. 30

3.4 Strip theory approximation of roll control effectiveness.[21] 32

3.5 Damping-in-roll moment coefficient for asymmetric wing variations at 15, 20 and 25 m/s flight speed. 34

3.6 Damping-in-roll moment coefficient for symmetric wing variations. 35

3.7 Roll power for VSW. 35

3.8 Roll rate variation for a flight speed of 15, 20 and 25 m/s. 36

3.9 Results of the roll rate for the VSW. 36

3.10 Roll rate available for the original wing with ailerons at 15, 20 and 25 m/s. 37

4.1 Pre-dimensioning variables of the VSW. 39

4.2 OMW glass fiber negative mould: the complete set (left); leading-edge detail (right). 40

4.3 Spar cross-section: circular on the inner wing (left); rectangular on the outer wing (right). 40

4.4 Rib sketch with the perforations to assemble both circular spar and rack-guide tube in the OMW. 41

4.5 OMW during assembly process. 42

4.6 Main spar configuration and position on the IFW. 42

4.7 IFW construction: with the first and second layers of carbon fiber and porous PVC foam, respectively (left); with the final carbon fiber layer (right). 43

4.8 IFW final aspect. 43

4.9 Standard S3001 Futaba servo chosed for wing actuation.[24] 44

4.10 Representative diagram of the reduction gears system used in the actuation mechanism. 45

4.11 Assembled new servo-mechanism. 46

4.12 New fuselage bay area: in CAD/CAM sketch (left); in the real fuselage (right). 47

4.13 Actuator bay: original attenuator mounted on the actuator bay (left); attenuator used for bench testing (right). 47

4.14 Rendered image of the original actuator bay and IFW from CAD/CAM design. 47

5.1 Assembled VSW on UAV Olharapo's new fuselage. 50

5.2 Sandbags used for wing load testing. 51

5.3 VSW load test: with no load (top left); with 1G - 3 kg (top right); with 2G - 6 kg (bottom left); with 3.5G - 10 kg (bottom right). 51

List of Tables

2.1 UAV characteristics. 18

2.2 Input data at each semi-span section. 22

2.3 Reductions (in percentage) obtained with VSW from original fixed wing design. 24

4.1 Wing dimensions obtained from expressions 4.1. 40

4.2 Final dimensions for OMW and IFW spars. 43

4.3 Obtained reduction of each set of gears. 45

5.1 Mass of each element of the VSW system. 49

Nomenclature

a	Original z-axis coordinate
a'	New z-axis coordinate
A	Aspect ratio
AOA	Angle-of-attack
a_0	Two-dimensional lift-cuve slope
a_{0_y}	Local two-dimensional lift-cuve slope
b	Wing span
b'	Left semi-span
b''	Right semi-span
c	Wing chord
c	Distance from the neutral axis
C_{Dfus}	Drag coefficient of the fuselage
C_{Dwing}	Drag coefficient of the wing
C_D	Drag coefficient
cg	Center of gravity
C_l	Airfoil lift coefficient
C_L	Wing lift coefficient
C_{l_p}	Dimensionless damping derivative
C_{l_y}	Roll control power in terms of span extension
C_{l_α}	Airfoil lift-curve slope
$C_{l_{\delta_a}}$	Section roll control power
$C_{L_{\delta_a}}$	Wing roll control power
C_M	Pitching moment coefficient
D	Drag
d_{ribs}	Distance between ribs in the outer moving wing
D_{wing}	Wing drag
I	Second moment of area of the cross-section
IFW	Inner fixed wing
l	Rolling moment
L	Lift

L/D	Lift-to-drag ratio
L_{fus}	Fuselage width
L_{rack}	Rack length
M	Bending moment at the section
M	Mach number
OMW	Outer moving wing
p	Angular velocity/Rolling rate
P	Required power
R	Length increment
S	Wing area
S_{rack}	Rack stroke
W	Aircraft weight
w_i	Angular velocity at each i gear set
w_m	Angular velocity at the motor
w_p	Angular velocity at the potentiometer
V	Flight speed
VSW	Variable-span wing
X	Inner fixed wing length
Y	Outer moving wing length
z	Original z-axis
z'	New z-axis
α_w	Wing angle-of-attack
δ_a	Aileron deflection
ρ	Air density
σ	Bending stress

I dedicate this work to my parents ***Joaquim*** *and* ***Isabel****, who always believed in me.*

Chapter 1

Introduction

Aircraft fly in a wide range of meteorological conditions, and under several flight regimes: take-off, landing, cruise, etc. An efficient flight in all these regimes requires different shape configurations. However, the bulk of aircraft are designed to have the best flight performance in its most important stage of flight, which depends on the mission that the aircraft has to perform. When the flight occurs outside the optimal condition, its performance is highly affected. Thus, being able to perform shape changes in order to optimize the flight envelope is highly desirable. This way, fixed wing aircraft make use of certain electro-mechanical or hydraulic mechanisms that allow them to change its aerodynamic wing shape in specific flight stages. These devices, that are activated when necessary, allow the control of the wing shape through sweep variation, airfoil curvature and wing twist, for example. Although significant geometry changes of an aircraft wing during flight may allow an approach to the optimal performance, very distinct missions, or multi-role missions are not possible with a fixed-geometry aircraft. The main role of a specific aircraft must be traced on plant, i.e., on the conceptual design. So, the development of new actuation equipment using adaptive structures, with or without smart materials, that could change many more geometric parameters during flight is much desired. This advancements would translate in a reduction of fuel consumption and an increase in maneuverability. Such highly versatile aircraft can in such a way be called *morphing* aircraft, because they make use of morphing solutions.

Morphing experiments have been made over the past years. The constant seek for perfection drew many distinct and interesting methods and concepts. In-flight change of airfoils characteristics, or wing planform shaping became the most sought solutions for morphing. Morphing solutions already presented are: variation in airfoil local camber, when the adaptive airfoil change its camber to obtain a desired lift thus eliminating the need for conventional control surfaces; variable-twist, when the wing is configured to

optimize the twist angle to obtain low-drag and high-lift aerodynamic characteristics; airfoil thickness distribution; wing sweep and span change, designed to change the aspect ratio of the wing; to name just a few. Inventive capability of its developers is almost endless. Therefore, a humble approach to the morphing problem is made in this chapter by presenting a development on the studies made so far, focusing on the particular aspects of each one, the assumptions made, and all the useful conclusions collected. Some of the studies produced good results, other did not, but all of them served to enlighten the path to follow.

1.1 Motivation

Morphing wing technologies have been a strong field of research and development in the past years. The design of adaptive structures, along with the research on smart materials, that allow bio-mimetic configurations on aircraft is highly desired. The new concepts and technologies developed are a constant attempt to enhance the performance of aircraft, making possible a new approach to the use of the aircraft and the multi-mission flexibility accomplishment. This performance enhancement capability was demonstrated in Tidwell's *et al.* work[1], where the Firebee drone base design was subjected to both airfoil and planform optimization for each flight stage and maneuvers. The positive results on the two optimization designs in comparison to the base design are plotted in Figure 1.1.

The development and recent increased use of unmanned air vehicles (UAV's), like the Firebee, for a wide range of both military and civil applications is due to the big potential of UAV's to perform distinct missions without direct risk to the crew, for its deployability and also for its low production cost. The use of such vehicles to test new concepts on performance enhancement is, therefore, the most logical choice. Morphing concepts include, mostly, ways to change aircraft shape in flight and the systems to perform those changes. Methods of airfoil and wing morphing include camber change, variable-twist, wing sweep change, and wing span change. An attempt on a more radical concept like wing morphing, rather than just airfoil morphing, is the intent of the present work. A variable-span morphing wing is designed to change its wingspan for various flight conditions to increase range. As a result of increasing the wingspan, the aspect ratio and wing area increase and the spanwise lift distribution decreases for the same lift. Thus, the drag of the morphing wing decreases and, consequently, the range of the aerial vehicle is increased.

The increase in aircraft performance is more than a good reason to develop new or give continuity to tested morphing configurations.

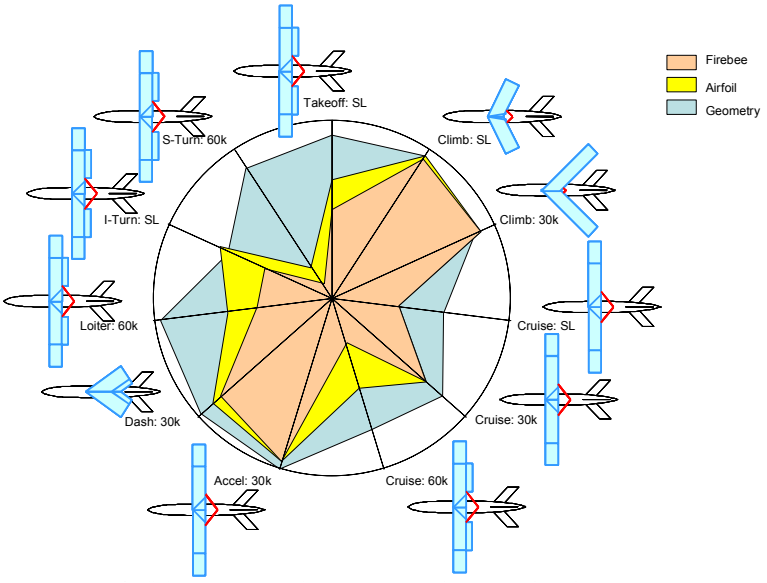

FIGURE 1.1: Spider plot comparing performance of the base-design Firebee, the morphing airfoil Firebee and the morphing planform Firebee.[1]

1.2 State of the Art

1.2.1 Telescopic Spars

Blondeau *et al.* from the University of Maryland, developed several studies in the morphing wing field in the past years. His research focused on the use of telescopic spars to actuate the wing while supporting structural wing loads. The pressurized telescopic spar could undergo large-scale spanwise changes and it was considered the key element of the projects. Several telescopic skins were used to preserve the spanwise airfoil geometry while ensuring a compact storage and deployment of the wing.

He began by showing that both range and endurance are strongly dependent on C_L/C_D and $C_L^{3/2}/C_D$[2], which are dependent on the wing aspect ratio. Clearly, an increase in wing aspect ratio resulted in an increase of both range and endurance. So, he concluded, "by tailoring the wing geometry one can adapt the lift and drag characteristics to a variety of missions".

The choice of the inflatable telescopic wing instead of a lead-screw mechanism to control the extension and retraction of the wings, which is the most studied actuation mechanism up to now, was due to the big increase in wing structural weight that results. Therefore, an inflatable system appeared less costly and more attractive, with a lot of advantages: light weight, compactness, compliance tailoring and minimal moving parts. The inflatable telescopic wing was composed of an aluminum telescopic inflatable spar with three elements and its extension/retraction control mechanism, length sensors, ribs

FIGURE 1.2: Pneumatic spars and root rib.[3]

fixed at the end of each section of the spar, fiberglass telescopic skins and a pressurized air source. The extension or retraction of the telescopic spar was controlled by changing the pressure in the chambers with a set of two miniaturized electronic-operated pneumatic solenoid valves. The feedback of the position of each moving spar element was given by two length sensors fixed at the tip. Both structural and dynamic performances were taken into account, concluding that the maximum allowable wing loading was 1532 Pa, and that with a pressure input of 6×10^5 Pa the spar could fully extend or retract in about 0,55 and 0,75 seconds, respectively. A smaller prototype of the spar was built to fit in the wind tunnel to be tested with the overall wing system.

Theoretical aerodynamic performance was calculated and compared with the final wind tunnel results. Two tests were taken into account: one with the wing fully retracted, which corresponded to a wingspan of 7", and another with the wing completely extended, corresponding to a 15" wingspan. The 7" wingspan test revealed that the telescopic wing had a higher lift coefficient and a lower drag than a rigid fixed wing of the same dimensions for all angles of attack, except for near stall conditions. The lift to drag ratio of the telescopic wing was also better, approximately 15%, than that of the rigid fixed wing, except near stall speeds too. A possible explanation for the increase in performance was purposed: less skin friction drag and a more flexible wing tip could result in such enhancement. However, the 15" wingspan test results were not even similar, with the rigid fixed wing out-performing in all aspects the telescopic wing. The fact that the lift to drag ratio was 25% lower than that of the fixed rigid wing could not be explained completely, although it was noticed that a considerable twist deformation at angles of attack greater than 5 degrees could have been the main cause to such low results.

The years have known further enhancements on the Blondeau's project. With the same structure concept, but with modifications, the results were slightly better. In the 2004's project[4], he used not one but two pneumatic telescopic actuators side by side, in order

to prevent the uncontrolled vibration of the wing and twisting verified in the earlier project. These actuators were coupled side by side by a rib at the tip of the wing and could not act independently, being capable to handle a wing load of about 718 Pa. The air pressurized system and valves were similar to the ones in the earlier project, with just some minor modifications in the extension/retraction system scheme. These changes led to a modification in the sensing system: a system of rack and pinion mounted on a potentiometer was added due to its simplicity and linear characteristics. A limited-number-of-turns potentiometer was used in detriment of an infinite-number-of-turns one avoiding counting the turns in the pressure control program, which was accomplished with a LabView Software program. The skins were made of fiberglass as in the first project and then glued to the ribs using epoxy resin. After wind tunnel testing for three different Reynolds numbers, four different spans, and angle of attack ranging from 0 to 24 degrees, it was possible to conclude that the solid wing was still generating more lift and less drag than the telescopic wing. It was claimed that the flexibility of the wing was still responsible for such poor results, because as the angle of attack increased, the lower surface of the airfoil could potentially be deformed by pressure, although it was not consistently observed. It was so concluded that the reduction in aerodynamic performance was due to the smoothness of the skin and possibly the seams of the wing sections.

These problems were not completely overcome when, in 2007, with their third project[3] on the matter, Blondeau and Pines proposed covering the seams with a thin aluminum foil tape to seal the seams in a static study, and then adding some friction tape in an area where the boundary layer should be and remain attached, and identify its impact on the aerodynamic performance. The friction tape was meant to facilitate the deployment/retraction of the pneumatic telescopic wing, particularly in the leading edge, where increased friction between wing elements was identified. In order to compare results, the solid wing was tested with the friction tape laid spanwise on its surface, in the same pattern as in the telescopic wing. All the tests were also performed without the friction tape. The results were conclusive: when the seams were covered, lift was improved consistently, and even more when approaching stall speeds, resulting in a higher L/D at almost all speeds, compared to the telescopic wing without the covering. However, friction tape seems to have no effect on aerodynamics performance. Despite the better results with the seams covered, the aerodynamic performance of the telescopic wing without the aluminum covering suffered of parasitic drag due to the seams of the wing sections and of a softer skin, resulting in worst results than those of a solid wing under the same circumstances.

Gamboa *et al.*[5, 6] recently presented the design of a morphing wing concept for an experimental UAV. In order to improve the vehicle's performance a multidisciplinary

design optimization tool was used to obtain a set of optimal wing shapes for minimum drag for a range of flight speeds. The aerodynamic shape optimization code used a 2-dimensional panel method formulation coupled with a non-linear lifting-line algorithm and a sequential quadratic programming optimization algorithm. The morphing concept was based on both wing planform and wing section shape with an extending spar and telescopic ribs mechanism. The skin material, natural rubber, chosen to allow high strains was not the best choice, since the reductions in wing drag obtained in aerodynamic optimization were not accomplished due to the flexibility of the skin. However, it was concluded that some improvements on the concept may lead to good results.

The automotive field had known also some experiments concerning telescopic wings using telescopic spars. In 1997, Czajkowski *et al.*[7], describing the results of NASA's SBIR Phase I program, determined the feasibility of a composite telescopic wing for a roadable aircraft. The half scale functionality model consisted of three segments, and was representative of one quarter of the wing. The main system was composed of two aluminum tubular telescopic spars, three skin/rib sections, a drive mechanism using a 12V motor for actuation, and a center box made of glass fiber and balsa wood sandwich plates. Preliminary structural analysis with NASTRAN and functionality model showed that telescopic principles were practical for deployable highly loaded airfoil structures. Some studies gave continuity to this kind of projects, although none of them with concrete feasible solutions.

1.2.2 Inflatable Wings

Morphing experiments concerning large span changes continued through several paths, testing the inventive capacity of its developers. The resilience and survivability of inflatable components manufactured from engineered materials had been long proved in missions like Pathfinder and MER, and in automotive impact attenuation airbags. Such flexible composite materials allowed the inclusion of embedded components to increase performance, like camber morphing.

Cadogan *et al.* developed several extensive studies concerning inflatable deployable wings. A review on the significant advancements on deployable inflatable and rigidizable wing structures for UAV and other airship applications was presented in 2003.[8] Wing warping to provide roll on inflatable wings was the focus of another work.[9] To achieve changes in camber section (with high response frequency, low power consumption, high life cycle, among other characteristics) several actuation methods were considered: piezoelectric actuators, electro-active polymers, shape memory alloys, pneumatic chambers, nastic cells and distributed motor-actuator assemblies. Another study[10] on

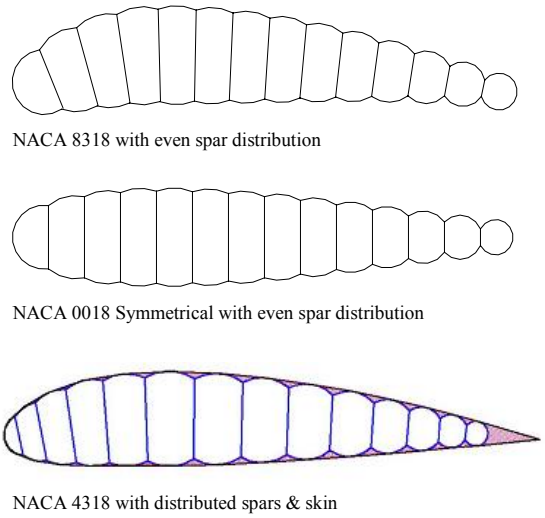

FIGURE 1.3: Inflatable wing cross-sections.[8]

a system capable of compact packaging for easy transportation and large damage tolerance as the main objectives was developed. Aspect ratio morphing was considered for packed systems which were air dropped or gun launched and deployed wings in flight, and for bigger vehicles requiring changes in aspect ratio to increase endurance. The study evaluated several materials such as unsupported films, film bladders supported by textile restraints and coated fabrics. A great advantage of inflatable wing structures concerned the manufacturing in close approximation to any wing shape, even those with camber. The so called "bumpy" surface improved aerodynamics for small Reynolds numbers (Re<500 000), with the possibility of a covering being added if required. The work included several technology studies about camber morphing (wing warping) through embedded devices, aspect ratio morphing, concealment through structural materials development, system durability and "disappearing materials". For wing warping Shape Memory Alloys (SMA), Electro-Active Polymers (EAP) and servo actuated systems were considered. But since SMA were readily available and had the necessary stress and strain response, they were selected for the study. The density of the wires per inch of the wing surface was varied in each case. It was observed that the decrease in the SMA wire diameter led to shorter response time from thermal activation and cooling. A servo mechanism was added to the SMA wires, achieving quick response times with significant wing deflection – closer to that of a wing flap arrangement at the trailing edge. Both configurations, SMA and servo mechanism, were flight tested.

The aeroelastic behavior of the inflatable wing – mainly twisting and bending – was determined through wind tunnel testing. The leading edge suffered the largest deflection – approximately 32 mm, which was within typical design values of tip deflection under flight loads. The 2 degree maximum wing twist registered was also within acceptable

FIGURE 1.4: SMA wires integrated on inflatable wing.[10]

values. Both roll moment coefficient and aileron control power were determined by comparing the warping wing with traditional ailerons, for an inflatable wing with an externally mounted servo mechanism. A rigid aileron of similar chord-wise length was used, in the same profile, for comparison. It was observed that the inflatable wing exhibited a higher roll moment coefficient for the same flap deflection angle than the rigid wing. Although, in terms of aileron control power, the advantage went to the rigid wing, with $9.9/^{o}$ to $4.0/^{o}$ of the inflatable wing.

A series of controlled tests were conducted to evaluate the survivability of a coated fabric wing used in the MIAV UAV prototype, and a bladder & restraint design – consisting of a thermally welded urethane bladder and a sown Vectran textile restraint. The tests included rapid deployment (0.4 seconds), a 23 kg shot bag drop on the tip and at the center of the wing, rapid inflation from a high pressure source and flight impact tests – crashing into many surface types. The pass criteria was no change registered in leakage, which was achieved in all tests. Hence, it was concluded that inflatable wings registered a high impact survivability, reusability and packability, and actuated as impact absorbers to other components of the aircraft. The inflatable nature of the wings granted them a robust behavior that allowed an expanded flight envelope and less proficient piloting.

Jacob *et al.* also presented a series of works on inflatable wings. A successful high-altitude test was performed[11] to demonstrate the feasibility of rugged inflatable wings for planetary exploration. The wings were deployed at 29261 m, reaching a maximum altitude of 29866 m, being descended with parachute recovery system. The potential for multifunctional inflatable structures with power generation capabilities was demonstrated by mounting flexible solar cells on the wing surface. A detailed finite element model of warping Vectran inflatable wings was presented[12] to analyze the effects of aerodynamic loading and also to explore design options for warping actuation. Inflatable material properties were determined with laboratory tests. The finite element model was validated using results of static cantilever wing bending and twisting loads

applied at the tip of the inflatable wing. The advantages (stowability and robustness) and disadvantages on the use of inflatable wings on UAV's was discussed on a recent work.[13]

A different approach to aspect ratio morphing during flight using inflatable wings was addressed by Kheong and Jacob[14] last year. The study was carried out for a polyurethane fabric inflatable rectangular wing, with a 36-inch semi-span from tip to root and chord of 13.5 inches. The inflatable wings were attached to both ends of a rigid wing – using an NACA 4318 airfoil – with an 150% increase in aspect ratio. Two concepts were generated: an aspect ratio morphing concept using an inflatable wing with folding mechanism, and a simpler one using just an inflatable wing – although, only the last one was used in the study due to its less expensive and less complex structural design. The inflatable wing was designed for an internal pressure of 55158 Pa and did not had any control surfaces – therefore, wing warping was used for roll control. The set was flight tested using both inflatable semi-span wings attached to a rigid wing at the end of the tip chords with silicon tape – which revealed acceptable for temporarily bonding the set. Two different flight configurations were performed: a dash configuration using the rigid wing – with both inflatable wings rolled up closely at the tip of the rigid wing; and a loiter configuration with inflatable wing pre-inflated. The light-weight pressure inflation system had a slow inflation rate; however, the lower overall aircraft structural weight and the reduced rigid wing strength due to reduced dynamic load (since high dynamic load was not experienced on the fuselage skin or rigid wing due to high speed deployments) could represent significant advantages.

Aerodynamic analysis was performed for the two aspect ratio configurations. The lift coefficient prediction for both configurations was calculated. A 58% increase in lift coefficient was estimated after the inflatable wings were deployed. It was observed that the high aspect ratio wing C_L/C_D was significantly higher than that of the low aspect ratio wing. The thrust required calculation showed a difference of 25% between low and high aspect ratios. The study showed also the benefits of high aspect ratio wing on the stall speed (achieving a reduction from 8.1 to 4.8 m/s), and in rate of climb, 16% higher at 15.24 m altitude than that with low aspect ratio configuration. After the flight tests, deployment tests were performed in the wind tunnel to verify the impact of dynamic pressure on the inflatable wing during the inflation process. Several cases with different deployment conditions and folding methods were tested; it was observed that all deployments took about the same time to reach the minimum pressure at 41368 Pa.

1.2.3 Stability Analysis

Blondeau *et al.* explored the effects of changes in aspect ratio on the stability properties[15] of UAV's. The study presented a stability analysis to prove that variable aspect ratio (VAR) wings maintain stability during symmetric changes in span. The analysis was made combining wind tunnel test results with a theoretical aerodynamic model.

He used the structure apparatus of the earlier project, a pneumatic telescopic wing with two pneumatic telescoping spars as actuators, and assembled it to a PVC simple wing-body model chosen for the wind tunnel test. Both telescopic half wings were mounted to the fuselage in a mid-wing configuration in order to place the zero-lift line coincident with the fuselage's x-principal axis. The major purpose of the wind tunnel test was to quantify the effect of differential span on the roll and yaw moment coefficients. Nearly fifteen tests were devoted to asymmetric span configurations.

The wing-body model was tested at free stream velocities of 8.94, 11.18 and 13.41 m/s with angle of attack ranging from -2° to 24° with ten different span configurations. Because the model had inherent static longitudinal and directional instability, it was necessary to add horizontal and vertical tail data to the wing-body wind tunnel data in order to perform dynamic stability analysis. Therefore, a correction of wind tunnel data for static stability has been made.

The theoretical aerodynamic model was based on finite wing theory to predict the roll moment coefficients for asymmetric span configurations. Experimental results showed that prior to stall, at any given angle of attack, a VAR morphing wing generates more roll moment than conventional ailerons, which was proved already in other recent works. It was also concluded that VAR wing suffers from large amounts of adverse yaw, as the result of asymmetric profile drag produced, and that this adverse yaw could difficult the use of asymmetric span as a means of rolling because it is opposite to the rolling moment. However, he proved that the yawing moment coefficient is always significantly less than the rolling moment coefficient.

The next step in Blondeau's study was to discuss the changes in stability for symmetric span cases. He stated that "symmetric changes in span can be used to optimize UAV performance for a specific mission segment" and therefore he studied the stability of free response of a symmetric model. Beginning with the definition of the equations of motion of an aircraft in a lateral-directional situation, he observed that an estimate of the principal moments of inertia, I_x and I_z, with changing wingspan had to be made. Hence, he subjected the wing to a torsional pendulum test. In order to achieve a pure rotational motion an inclinometer was used to ensure that the axis of the torsional rod passed through the center of gravity as it migrated with the wing's changing span. The

determination of the wing's principal moments of inertia was accomplished by subjecting the wing to a torsional pendulum test for the 40-40, 60-60, 80-80 and 100-100 symmetric configurations.

In order to determine the stability derivatives, he used aerodynamic data from wind tunnel tests on the wing-body in conjunction with theoretical data from the horizontal and vertical tail to find trim solutions for each of the four configurations. He observed that, as the wingspan changes, new equilibrium values of angle of attack and airspeed must be sought. Because changes in span were expected to correspond to changes in airspeed at steady cruise conditions, the trim angle of attack was fixed. Therefore, trim airspeed had to be changed as the span changed, so the available lift at a particular speed could balance the weight. Dimensionless stability derivatives were evaluated using Advanced Aircraft Analysis Program®, a software by DARcorp.

Finally, Blondeau *et al.* concluded that the VAR UAV was dynamically stable in the dutch roll and roll modes for the symmetric span configurations and that an increase in total span decreased the time constant, increasing therefore the damping of the dutch roll mode, making it more stable. They concluded also that the roll mode becomes more stable when increasing the total span and that asymmetric span configurations generate roll moments that can be used to control roll maneuvers.

Henry and Pines also presented a simple mathematical model[16] for an aircraft performing a pure roll by means of span morphing. They observed that, for a morphing wing, the standard six-degree of freedom model that describe aircraft dynamics should be revisited because inertial changes still appeared in the body axes and could not be considered negligible. This was due to the variable geometry in body axes, it was concluded. Therefore, after deriving the complete morphing moment equations from the baseline moment expressions, and considering the special case of a steady roll, it was possible to develop simple expressions for these inertial changes – or perturbations, meaning additional terms introduced into the dynamic equations by morphing. Having derived the full inertia-based equations and simplifying them to the case of a pure roll, aerodynamic effects were incorporated into the roll moment equation and compared with those of a conventional aircraft with ailerons.

The comparison between the variable-span morphing wing (VSMW) and the aileron differential equations showed that the span extension induced a damping roll moment greater than that due to aileron deflection and, thus, achieved the steady state faster. In fact, aircraft using VSMW for roll control achieved a larger steady state roll rate in approximately the same time as one using ailerons. Examining as well the damping terms in the two models obtained, it was possible to conclude that, for the VSMW, the magnitude of the damping coefficient increased as the span differential increased. These

results were a consequence of the conservation of angular momentum. The increase in span decreased the rate of roll, whereas decreasing the span tended to speed up the roll rate. In the case of the aileron, it was expected of the dimensionless damping derivative C_{l_p} to be independent of the angle of aileron deflection because it depended only on the taper ratio and the lift curve slope.

In the study, it was assumed that the aircraft *cg* location was fixed with the wing *cg* free to move. Because morphing causes the aircraft *cg* to migrate along the y-body axis, it was concluded that further work needed to be done to determine the effect of a migrating center of gravity on stability.

1.2.4 Aerodynamic and Aeroelastic Analysis

Bae *et al.*, from Virginia Polytechnic Institute and State University, in Blacksburg, proposed an application study[17, 18] of a variable-span morphing wing (VSMW) on a cruise missile as a means to increase range. He discussed the advantages and disadvantages of a VSMW applied to a long-range missile. The wings of the cruise missile should be anti-symmetrically changed to allow roll control, instead of conventional roll control fins. The major disadvantage was that the wing-root bending moment would be considerably high and so requiring a very high wing stiffness.

Aerodynamic characteristics and the range of the morphing wing were analyzed as the wingspan changed. The study used a subsonic doublet-hybrid method (DHM) panel code for the computation of subsonic aerodynamic forces. MSC/NASTRAN was used to model the wing-box structure of the morphing wing.

The VSMW had a root-chord length of 0.51 m and a wingspan of the original conventional wing of 1.0 m. The sweep angle of the leading-edge was 5.71 degree and the taper ratio 0.6. The wing area of the original wing was 0.413 m^2 with an aspect ratio of 5.0. When fully extended to 50%, the aspect ratio was 8.18 and the wing area 0.568 m^2.

The aerodynamic model of the VSMW for the DHM code used a 10×20 mesh for the conventional wing. When fully extended, the aerodynamic mesh was 10×30. DHM was used to estimate the relationship between the pressure difference at the doublet point and the downwash at the receiving point using the Kernel function. The structural model of the VSMW was composed of two wings: a main wing-box and a moving one, which extended from the main wing. The main wing and the moving wing were composed of four and two wing-box sections, respectively. In the two models, the moving wing-box was constrained to the main wing using the Multi-Point Constraint elements of MSC/NASTRAN.

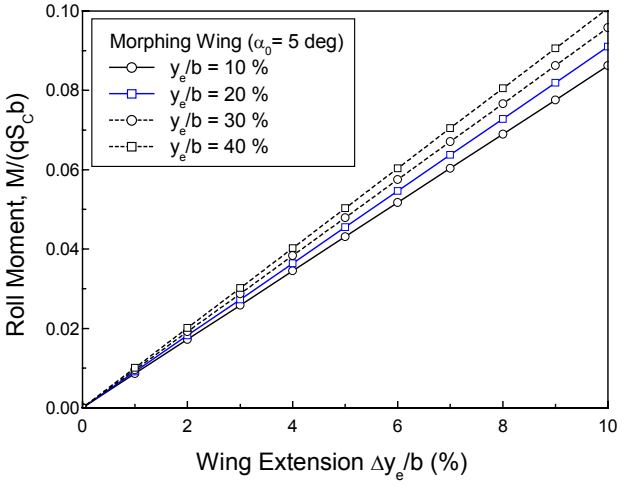

FIGURE 1.5: Roll moment due to asymmetric span control.[17]

The aerodynamic study[18] concluded that, for the same wingspan and angle of attack, the lift coefficient at M=0.7 was larger than that of M=0.0, and also that the lift coefficient of the morphing wing increased linearly as the wingspan increased. In fact, when M=0.7, the lift coefficient of the 50% extended wing was 1.6 times that of the original wing.

The wing load distribution tests revealed that for a M=0.0 and a lift coefficient of 0.4, the angles of attack of the morphing wing were 3.74, 2.30 and 1.72 degree for the 0%, 30% and 50% span-extended cases, respectively. It was demonstrated that torque at wing root decreased considerably as the wingspan increased, whereas the torque at wingtip increased only slightly. The main conclusion was that the VSMW did not require larger wing torsional stiffness as compared with the conventional wing and that the wing twist could be neglected in the design of the morphing wing. On the other hand, the bending moment of the morphing wing increased considerably as the wingspan increased, as expected. The contribution of the moving wing to the bending moment was very large, although the spanwise lift decreased. It was observed that the bending moment along the wingspan of the morphing wing was much larger that that of the conventional wing. So, the conclusion was that the wing deformation of the VSMW due to bending is much more significant that that due to torque. The aerodynamic study also revealed that the increase in wing area increased the profile drag, decreasing the induced drag. It was verified that the total drag of the morphing wing decreased 25% and the range increased 30%. The increase in range is an important advantage of a VSMW, as well as the control of the roll motion without conventional control fins, it was concluded.

The aeroelastic study[18] included the estimation of deformations due to aerodynamic forces, and divergence speeds. The flight condition used to calculate the aerodynamic

deformations of the VSMW was a M=0.0 and a lift coefficient of 0.4, and using the modal matrix obtained from the free vibration analysis and DHM code, the aerodynamic influence coefficients and the aerodynamic forces were calculated for each angle of attack. It was observed as expected, that aerodynamic deformation increased as the wingspan increased; this was mainly due to the increase of the bending moment. With 50% span-extended wing, the aerodynamic deformations increased dramatically – the wingtip deformations of the 0% and 50% span-extended wing situations were greater than 10% of their wingspans when the dynamic pressures were 40 kPa and 15 kPa, respectively. The divergence dynamic pressure was calculated from an equation derived from aeroelastic equations of the wing, and it was found that at 50% span-extended wing this pressure was 30 kPa at M=0.0. This way, it was concluded that VSMW aeroelastic characteristics become worse, and it was important a further investigation on static aeroelastic stability.

1.2.5 Fully Adaptive Model

Neal *et al.* designed and constructed a large scale shape change fully adaptive aircraft[19] which was used as an experimental testbed for aerodynamic modeling and flight control. It was possible, along with five independent planform changes (increase in span and sweep variation for each wing, and tail extension/contraction to control the aerodynamic center location) to have independent twist control for each wing. The wing and fuselage were designed from modified NACA 0020-64 and NACA 0017-64 airfoil sections, respectively. On each end of the fuselage, the extruded section tapped down to a smaller chord NACA 0020-65. Two rotational actuators for wing twist and five linear actuators to control wing shape – pneumatic actuators for tail and wing extensions (large strokes), and a lead-screw mechanism for sweep actuation were used. The control and data acquisition circuit used PC/104 boards and a Matlab/Simulink environment. The complete *apparatus* can be seen in Figure 1.6.

The 7-DOF experimental model was tested in wind tunnel to evaluate the aerodynamic characteristics, with particular focus on the aerodynamic center location and the drag force. It was found that, for a span extent of 0%, 50% and 100% the aerodynamic center shifted 19.5%, 22.3% and 25.7%, respectively. To assess the influence of the planform variation on aircraft stability, it was determined that the *cg* variation was 11% from an unswept condition to a fully swept one. This indicated that, increasing the sweep, the aircraft became more stable.

It was observed that the change in C_{l_α} was less sensitive to sweep changes than the aerodynamic center. The drag polars were calculated for the unswept and fully swept configurations in order to find the influence of planform variations on drag. It was

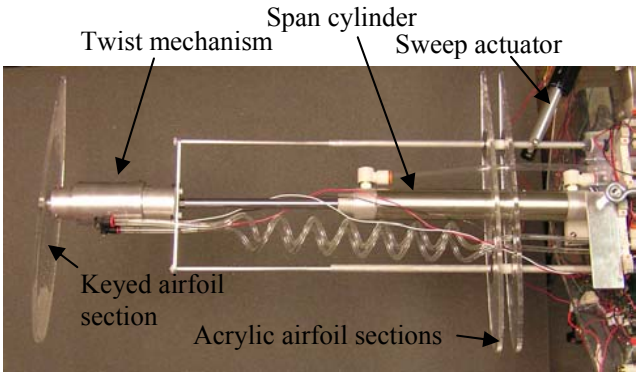

FIGURE 1.6: Extended wing section showing the three bar segment.[19]

concluded that 0% span-extent cases had minimum drag at low C_L values, while 100% span-extent cases had minimum drag at high C_L values. The two major effects of sweep on the lift and drag appeared to be an increase in both the minimum C_D and the maximum $C_L(C_{L_{max}})$ for the fully swept case. The increase in the minimum C_D for the fully swept case was likely caused by the wing tips acting as trailing edges as the sweep increased. It was observed that, unexpectedly, that $C_{L_{max}}$ was higher for the swept case. C_L and C_M vs. angle of attack were plotted and was possible to see a "break" in the C_M curve for both swept and unswept cases at the same angle of attack. C_L for the unswept case broke much earlier that for the swept case which indicated that, although flow separation occurred at the same angle of attack for the two cases, the swept case obtained more lift on the inboard section of the wing and on the fuselage.

1.3 Objectives

The objectives of the work are the design, conception and validation of an experimental telescopic span wing, actuated by a simple rack and pinion electro-mechanical system, for application on the UAV Olharapo. Aerodynamic analysis and optimization must be performed in order to enhance its flight performance over a specific flight speed range. Thus, optimization computational tools must be modified to fit the wing's requirements and work goals. A numerical analysis on aircraft's roll authority must be performed to determine the roll rate available with asymmetric span control. A wing must be designed and constructed in order to implement the actuation system while, at the same time, being able to be installed on the aircraft under study. A simple actuator that provides the required span variations must be studied, constructed and implemented on the wing's final assembly. The final prototype (wing plus actuator) should be an attach-and-go system, i.e., must be detachable from the plane without complexity, like

a complete independent UAV equipment. The project budget must be as limited as possible. The next topics must be accomplished in order to achieve the goals described:

i) Review of the most successfully tested mechanisms on UAV span morphing in order to retain the best working ideas and trace the path of the project;

ii) Learn how to work with the optimization computational tool designed by Dr. Pedro Gamboa for optimal performance wing design. There are some modifications in the source code that must be performed to admit new geometry parameters contemplated in morphing span wing design;

iii) Build a simple computational code to perform roll control analysis, allowing for the variations in the lift distribution occurring when wing tips are actuated. The code must contemplate both symmetric and asymmetric span variations;

iv) Design a large scale span change morphing wing and the actuating mechanism with CAD/CAM tools, attending at the aerodynamic optimization results and available materials;

v) Build both wing and actuator using conventional materials available in the department's workshop;

vi) Bench test the assembled telescopic wing.

1.4 Dissertation Layout

The thesis begins with an introduction on morphing concepts and with particular focus on large scale span change studies and experiments. A separation between the distinct concepts on wing morphing is made: wing span change, wing twist, camber change and wing sweep change. A short review on stability and aerodynamic/aeroelastic studies is also performed.

The dissertation is divided into four main parts: aerodynamic analysis (Chapter 2); rolling rate analysis (Chapter 3); system design and construction (Chapter 4); and wing testing (Chapter 5). Each of these chapters has a concluding section.

Chapter 2 presents the aerodynamic analysis and shape optimization process for minimum drag of a morphing wing in a specific flight speed range of an experimental UAV. A description of the optimization and analysis models used is made.

Chapter 3 presents a static stability analysis using a computer code in order to obtain damping-in-roll moment coefficient and roll moment available at a given flight condition, ranging both flight speed and symmetric/asymmetric span variations.

Chapter 4 presents a detailed exposition of the overall system design using CAD/CAM tools, sizing of the several parts that constitute the wing, including the actuation system and actual construction.

Chapter 5 describes the overall assembly of the morphing wing and the results of bench testing are presented.

Chapter 6 presents the overall conclusions as well as future work and recommendations.

Chapter 2

Aerodynamic Analysis

2.1 Aircraft Characteristics

The aircraft in study is called Olharapo, and is an experimental UAV developed by the Aerospace Sciences Department, at University of Beira Interior. It is a high-wing push configuration, with the propeller placed behind the wing, at the beginning of the V-tail. The original wing structure is made of balsa wood ribs, a balsa wood torsion box and hard wood spars. The takeoff weight of the aircraft, W, is 60 N. The original wing has a constant chord, c, of 0.25 m across the span and a wing area, S, of 0.625 m^2. From c and S one can calculate the wing span, b, and the aspect ratio, A. UAV data is presented in Table 2.1. The airfoil used is a SG 6042, a low speed airfoil with a good compromise between maximum lift coefficient and design simplicity. The cruise speed of the aircraft is about 15 m/s, and maximum speed about 25 m/s. The main goal of the project is to design a telescopic wing with minimum drag over the same range of flight speeds. A new fuselage has been designed to increase aircraft's cargo area, and therefore, the telescopic wing is designed and intended to be assembled onto the new fuselage. Despite the change, the characteristics of the old fuselage were maintained in the new one, so the aircraft data did not suffered significant changes. It is assumed that only the wing contributes to lift.

In the aerodynamic analysis and optimization the drag coefficient of the fuselage, C_{Dfus}, is assumed constant with a value of 0.015. The wing's drag coefficient, C_{Dwing}, is a function of the wing geometry, angle of attack and speed for a total lift equal to the

W, N	S, m^2	c, m	b, m	A
60	0.625	0.250	2.500	10.000

Table 2.1: UAV characteristics.

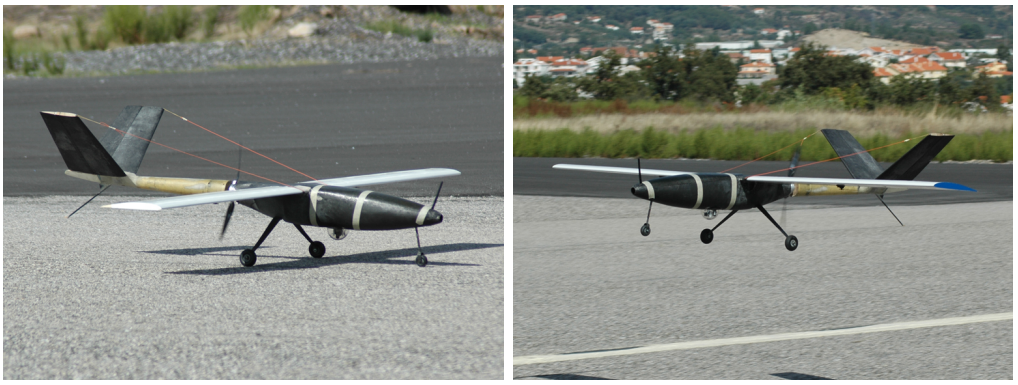

FIGURE 2.1: UAV Olharapo.

vehicle's weight. The UAV has an electric brushless outrunner motor Flyware PowerREX 430-700 with 1221 W, driving a 13"x6" fixed pitch propeller.

2.1.1 Performance Requirements

The main goal of this project is to have a wing that can perform in-flight span variations, a variable-span wing (VSW), in order to maximize its performance at a given flight speed. A constant flight altitude, namely at the sea level, was assumed. The aircraft should be capable to operate in the same range of speeds as with the original wing, from about 12 m/s to 30 m/s, although enhanced performance is expected, i.e., improved range and endurance.

2.2 Aerodynamic Optimization

2.2.1 Shape Optimization Tool

The main purpose in the design of the VSW is to enhance wing performance by minimizing the wing drag, D_{wing}, at a given range of flight speeds in a cruise condition, when lift, L, equals the aircraft weight, W. In order to seek the best performance, a computational tool developed by Dr. Pedro Gamboa in a recent work[5] was used. This tool searches for the best airfoil geometry and wing planform by taking into account several geometric constraints. However, in this case, the airfoil was kept fixed and a rectangular planform wing chosen due its simplicity and to allow a comparison to the original wing of the UAV. It also has to be noted that a low speed aircraft like UAV Olharapo hardly requires any sweep, or even any wing dihedral, because of its highly stable, high-wing configuration.

The aerodynamic analysis is performed in two main steps. First, using the solver of the XFOIL code, the 2-dimensional aerodynamic coefficients as functions of the angle of attack and Reynolds number at previously specified sections across the span are obtained. In the present work four sections all over the span were defined, where the first set is representative of the inner fixed wing (IFW), with a bigger chord, and the second of the outer moving wing (OMW), with small chord. XFOIL code represents the inviscid flow using the steady integral form Euler equations, and represent the boundary layers and wake recurring to a compressible lag-dissipation integral method. A surface transpiration model allows proper calculation of limited separation regions. The airfoils are represented by b-spline control points, used to define the airfoil camber line and the airfoil thickness distribution, which are combined to give the airfoil surface. In the second step a non-linear lifting-line method algorithm is used to obtain the lift distribution and the induced drag. Integration of the airfoil drag over the wing span gives the parasite drag. Wing representation is done by the chord and incidence at specified sections along the semi-span. The sections' aerodynamic information comes from the previous step. Due to morphing wing simplicity design, the lifting-line method was considered accurately enough to estimate the 3-dimensional aerodynamic coefficients of the wing. In this aerodynamic analysis it is assumed that the wing remains planar after loading and so spanwise loads are not predicted.

Aerodynamic shape optimization is performed by a sequential quadratic programming (SQP) constrained optimization algorithm FFSQP, version 3.7, whose purpose is to minimize a differential real function subject to inequality and equality constraints. The gradients of the objective function are computed using forward finite-differences, enabling the problem of finding gradients to be treated as a black box, and allowing the algorithm to be used with any fluid flow solver without the need to change the solver's code. The flow chart in Figure 2.2 illustrates the implementation of the aerodynamic shape optimization tool.

2.2.2 Input Data Requirements

The input data of the wing shape optimization tool was based on the aircraft characteristics and on some assumptions made. A crucial starting point was the specification of the range of flight speeds the aircraft would operate in. Based on the aircraft data collected with the base fixed wing design, a stall speed of around 12 m/s and a maximum speed of 30 m/s were predicted. The range was extended from 10.75 m/s to 50 m/s to allow a direct comparison with the original fixed wing results. The increment on the flight speed varied from 0.25 m/s near the stall speed and predicted cruise speed (20 m/s), to 10 m/s from the cruise speed up to 50 m/s. Another requirement on the

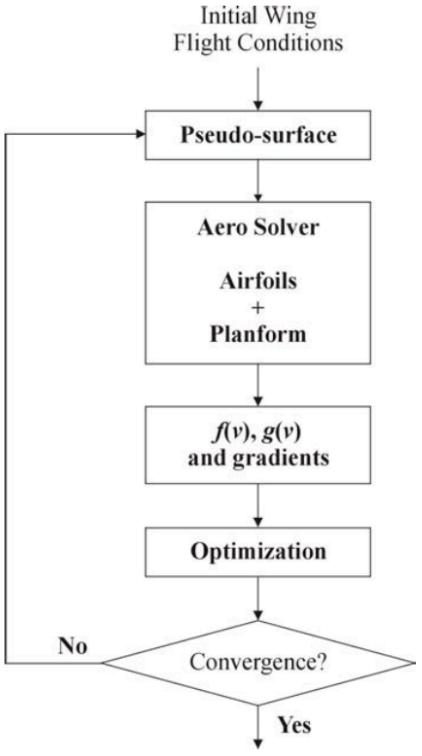

FIGURE 2.2: Flow chart illustrating wing aerodynamic shape optimization design tool process.[5]

optimization tool input data was the total weight, W, of the UAV. It was assumed that the new VSW should not be much heavier than the fixed one. So, the reference value for the weight was 60 N. It has to be noted that the total aircraft weight is calculated and updated if required by the optimization tool for a full extended wing configuration. This process was carried out by assuming a cruise condition where $L = W$. The total aircraft weight does not suffer any variation because, due to span variation, the mass is only moved from one place to another. In fact, this procedure was performed for near stall speeds, from 10.75 to 12 m/s, where the weight value converged to 60.65 N. Therefore, from 12 m/s and up, the aircraft total weight used was 60.65 N, with the weight update option turned off. This represents a 650 g mass increase in the VSW comparing to the original wing set.

It was necessary to define all the sections of the semi-span wing with the inherent constraints. The wing was rectangular, so four sections were sufficient to define the semi-span wing. The main objectives on the design of the VSW were: maintain the performance of the original fixed wing at low speeds, and increase the performance at higher speeds. That way, and in order to make a comparison between the original fixed wing and the VSW, the maximum allowable span was set to 2.5 m. Therefore, taking into account the fuselage width and geometric characteristics of the wing, the positions of the four wing sections were defined from the root to the tip.

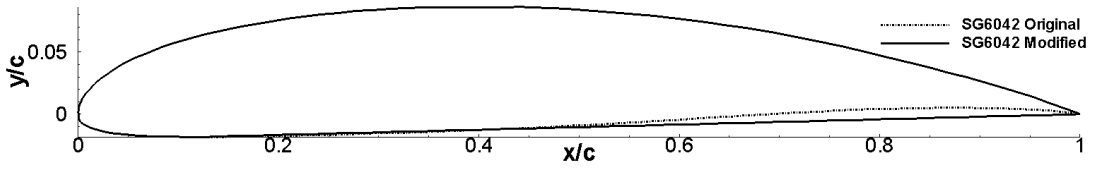

FIGURE 2.3: Comparison between airfoil SG 6042 original and modified.

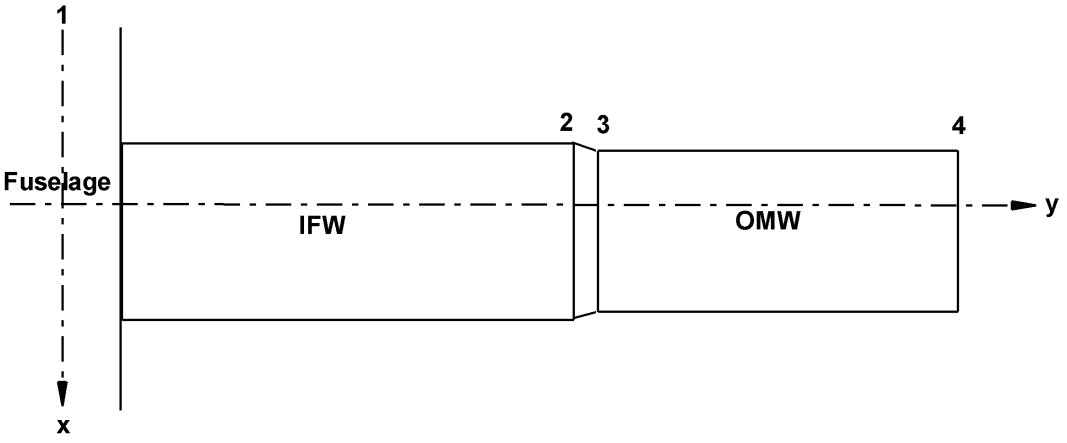

FIGURE 2.4: Schematic illustration of the variable-span wing.

Between sections 2 and 3 a small distance was needed because the aerodynamic analysis tool cannot define two different sections in the same y-axis coordinate. Section 2 and 3 define the separation between inner and outer wings. Section 4 was movable along the y-position axis. Its position varied from the y-coordinate of the section 3 to the maximum allowed semi-span length of 1.250 m.

Section	1	2	3	4
Position, m	0.000	0.700	0.725	0.725-1.250
c, m	0.283	0.283	0.250	0.250
$(t/c)/(t/c)_{ref}$	1.180	1.180	1.000	1.000

TABLE 2.2: Input data at each semi-span section.

The original SG 6042 airfoil from the fixed wing, which has a relative thickness of 10% and a 0.250 m chord, was slightly modified and applied to the inner wing. A straight line was drawn from the lowest point of the lower surface to the trailing-edge. The original and the modified airfoils are presented in Figure 2.3. The resulting airfoil is obviously less efficient than the original, but the modification allowed a smaller IFW airfoil. Since

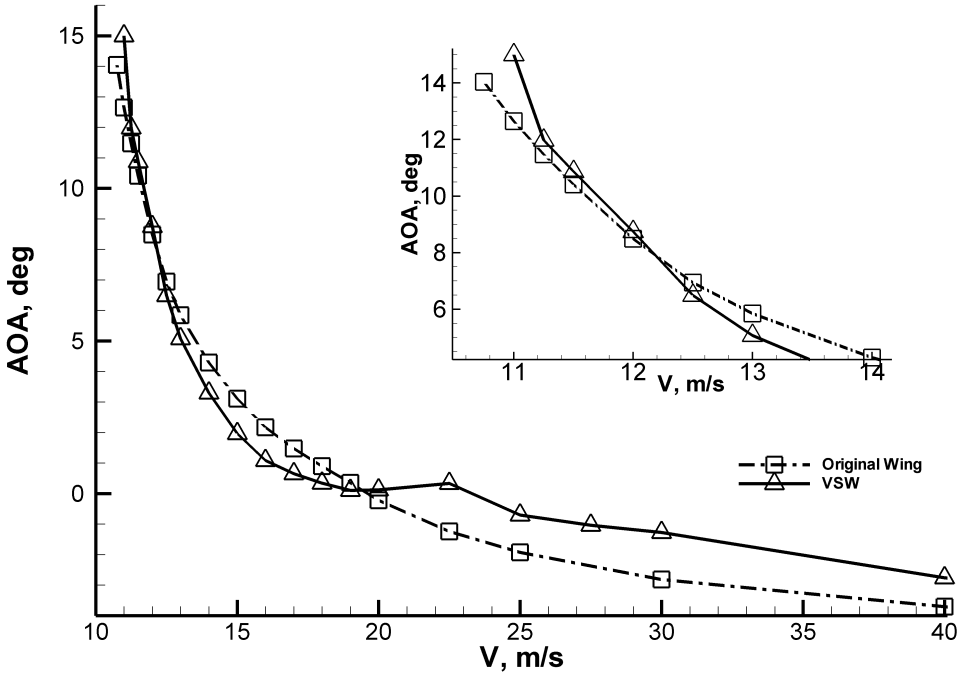

FIGURE 2.5: AOA variation with flight speed for both original and VSW.

IFW airfoil was achieved by offsetting the OMW airfoil, the curved lower surface, if present, would create big geometric conflict when the offset was performed. The trailing edge of the inner wing would eventually intersect the IFW. The resulting IFW airfoil has a chord of 0.283 m. Figure 2.4 presents the schematic variable-span wing used for the aerodynamic optimization. The summarized input data used to perform aerodynamic shape optimization is shown in Table 2.2.

2.3 Optimization Results

The original UAV fixed-wing was analyzed using the aerodynamic optimization tool. In this case, the only design variables were the AOA and the wingspan, since the rest of the geometric parameters were constant. The original wing, being rectangular, non-twisted and non-tapered, needed just two sections at the root and tip of the semi-span wing to define the wing model. The flight speed range used was the same as that used on the VSW analysis, to permit a comparison between the two. The objective of the analysis was to find an AOA and a wingspan at each flight speed in which the condition $L = W$ was satisfied. The aerodynamic results of the original wing *versus* the VSW are presented from Figure 2.5 to Figure 2.9.

The original wing exhibits, at cruise speed (20 m/s), a negative AOA, which shows that the wing is oversized for this flight condition. However, this situation allows a low

stall speed. In Figure 2.5 one can see that the VSW has better performance than the original wing at speeds above 22.5 m/s. At 30 m/s, the VSW has about 20% less drag than the original one. At speeds up to 40 m/s and 50 m/s, the drag difference increases drastically, 33% and 40%, respectively. At low speeds, the original wing outperforms the VSW, although presenting only slightly better results. The original wing was designed for low speeds, and near the design point it was expected to have better performance than the VSW because of the higher relative thickness ratio of the IFW airfoil and because the modified SG 6042 used in the VSW suffered a reduction in performance. Therefore, the IFW presents a slightly higher total drag at low speeds when the wing is full extended, which only is compensated at higher speeds, when the wingspan starts to decrease, reducing aspect ratio and total drag relatively to the original wing. This can be seen by comparing Figure 2.7 with the rest of the graphical results where the span reduction occurs. For example, one can see that at 22.5 m/s a major span reduction takes place, which is coincident to an increase in L/D ratio, clearly when VSW performance surpasses the original wing performance. Stall speed increased too, from 11 m/s in original wing to 11.25 m/s in the VSW.

The power required to satisfy a cruise condition ($L = W$) in the defined speed range for both original wing and VSW can be seen in Figure 2.9. It has to be noted that these values are for the wing alone; in reality, a non-lift contributing fuselage implies always losses in performance, and therefore, lower performance gains. From 22.5 m/s and up, the VSW surpasses the original wing. The accentuated span reduction at this speed (already commented above) and the decrease in the total drag due to the reduction in aspect ratio requires less power from the motor to maintain the flight speed.

% Reductions	15 m/s	20 m/s	25 m/s	30 m/s	40 m/s
Span	0.00	0.24	29.94	42.00	42.00
AR	6.88	15.34	36.62	48.55	48.55
Drag	-1.84	-3.41	5.03	18.28	32.93

TABLE 2.3: Reductions (in percentage) obtained with VSW from original fixed wing design.

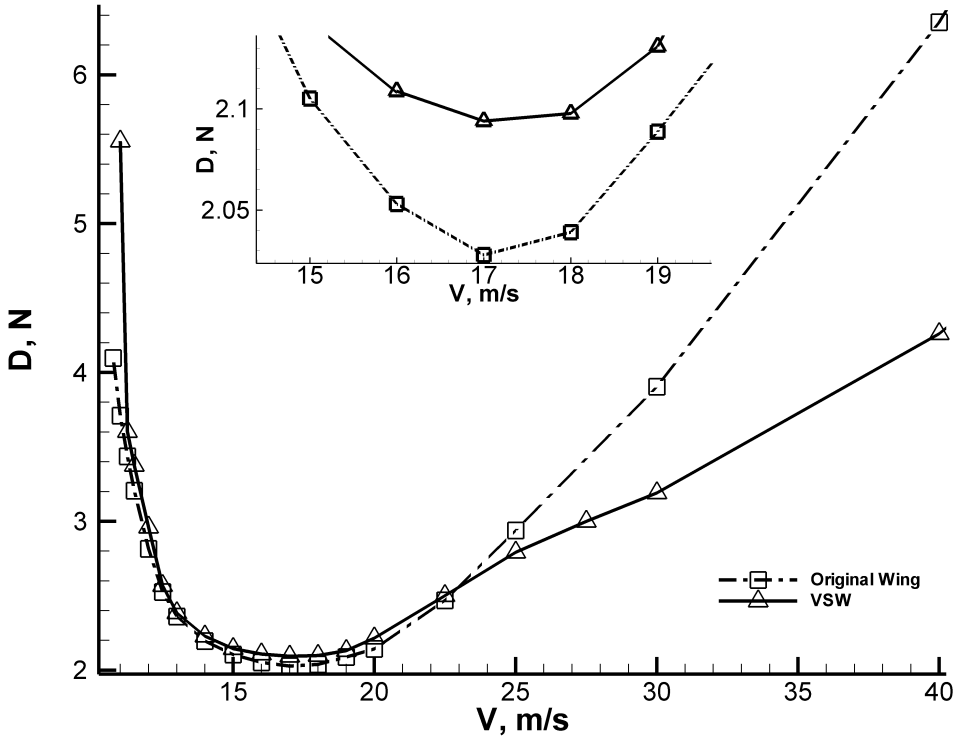

FIGURE 2.6: Drag comparison between original and VSW.

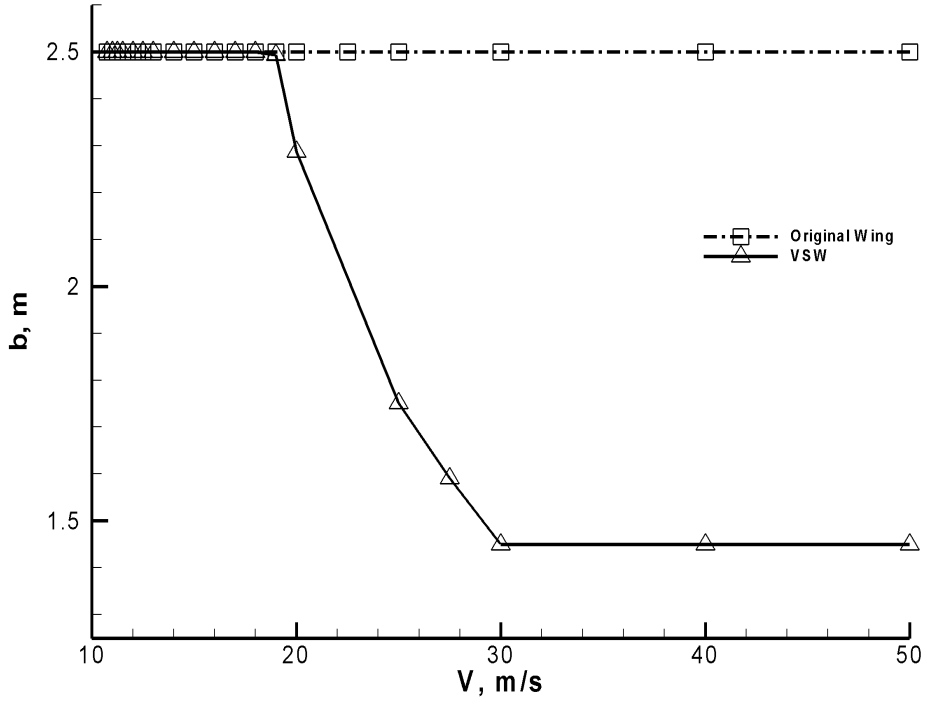

FIGURE 2.7: VSW span variation.

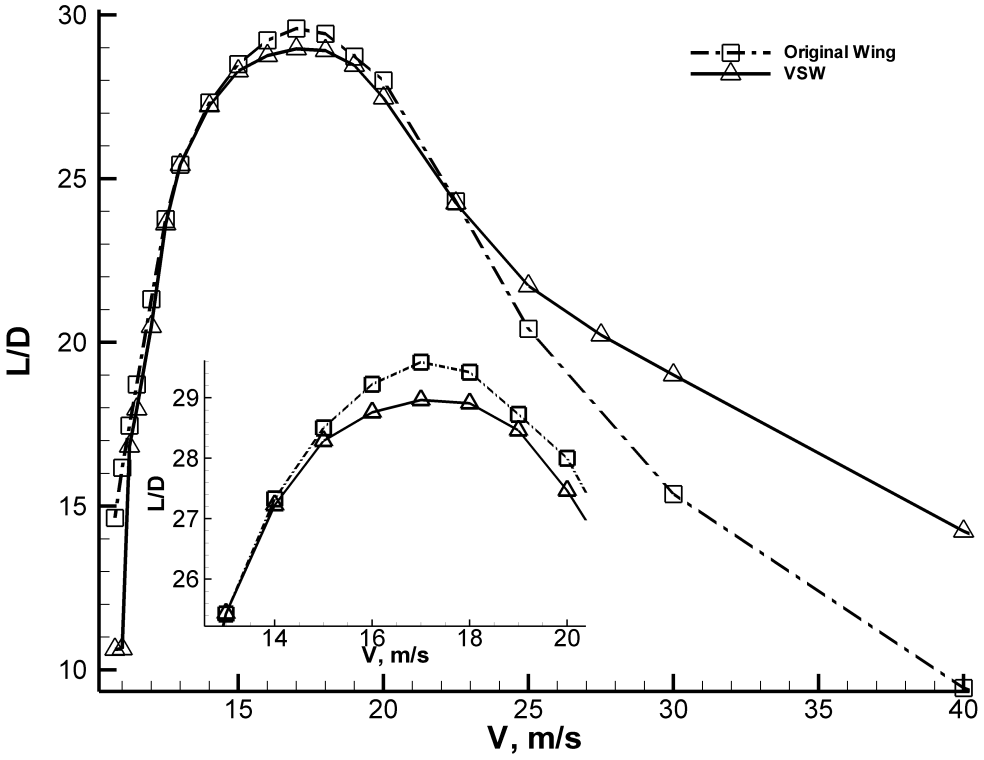

FIGURE 2.8: Lift-to-drag ratio comparison for both wings.

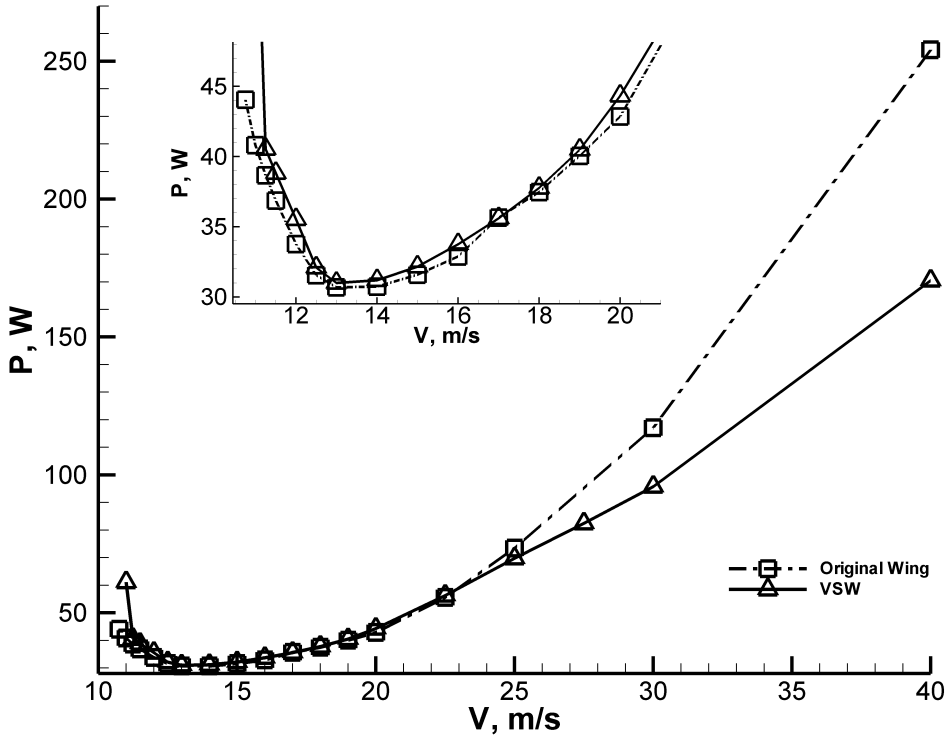

v

FIGURE 2.9: Required power variation with flight speed.

Chapter 3

Rolling Rate Analysis

3.1 Stability Concepts

Stability control on morphing aircraft is always a matter of paramount importance. The alterations on aircraft motion due to physical modification on structures and also the implication that in-flight large scale changes produce on stability must be taken into account. In the case of a telescopic wing, the ability to perform large variations in span waste the possibility to have high performance roll control through conventional ailerons. However, recent researches on the prediction of roll control by asymmetric span variation were carried out.[15, 16] It was concluded that roll modes become more stable with the increase in total span, and also that asymmetric span configurations generate roll moments that can be used to control roll maneuvers. Therefore, the use of ailerons in such wing configurations is not necessary. This leads to a simplification of internal and external wing design. A "cleaner" wing surface, without external moving parts, is always preferable. Hence, the study on wing stability, particularly for roll control, is an important aspect in telescopic wing design and cannot be neglected.

Some major aspects concerning lift distribution in morphing wings have to be made. Morphing wings in general suffer from variations on lift distribution that are not detected in ordinary fixed wings. In asymmetric span changes, and assuming an elliptic lift distribution, the center of the ellipse moves along with the wing. Therefore, the lift distribution symmetry point moves in the direction of the bigger semi-span aspect ratio, i.e., in the direction of the bigger span extension. For example, when the right wing registers a bigger span extension than the left wing, the lift distribution symmetry point will move also to the right. In this situation, this point does not coincide anymore with the longitudinal axis of the fuselage. The distance between the original aircraft center point and the new lift distribution symmetry point is not taken into account in

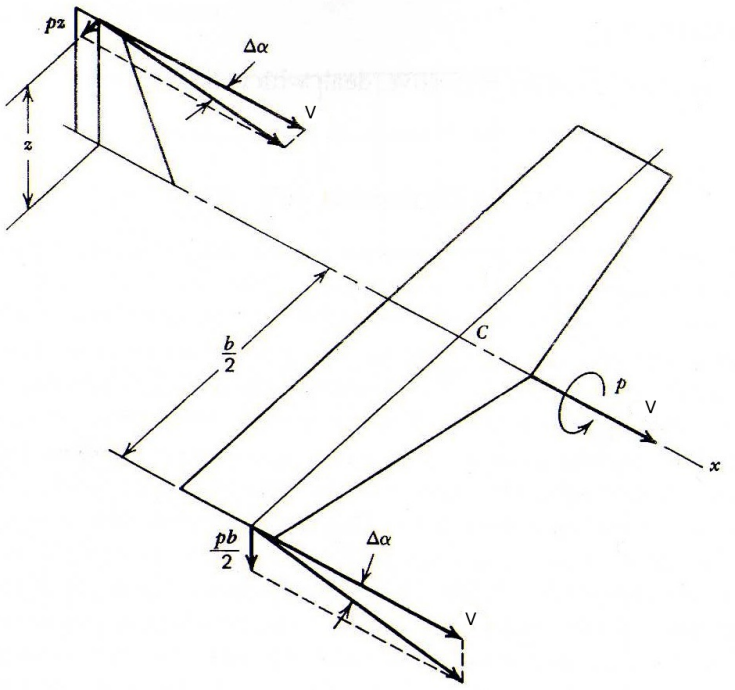

FIGURE 3.1: AOA changes due to angular velocity p.[20]

conventional stability derivatives expressions. The present calculation approach is able to perform this little correction on the lift distribution. For symmetric span changes, lift distribution will behave like a fixed wing and this issue is not relevant.

In order to estimate the roll moment of the VSW, it is necessary to estimate the stability derivatives (more exactly aerodynamic transfer functions) that influence roll motion. Since the telescopic wing has no dihedral, no sweep and no twist, and since the tail influence is not taken into account, the stability derivatives that matter for roll moment calculation are C_{l_p}, also known as the *damping-in-roll* derivative, and $C_{l_{\delta_a}}$, which expresses roll control power. C_{l_p} expresses the resistance of the aircraft to rolling. Except in somewhat unusual circumstances, only the wing contributes significantly to this derivative. The angle of attack due to the angular velocity about the x-axis, p, varies linearly across the span, from the value $pb/2V$ at the right wing tip to $-pb/2V$ at the left tip. The anti-symmetrical α distribution produces an anti-symmetric increment in the lift distribution as shown in Figure 3.2. In the linear range this is superimposed on the symmetric lift distribution associated with the wing angle of attack in undisturbed flight. The large rolling moment l produced by this lift distribution is proportional to the tip angle of attack $\hat{p}$, and C_{l_p} is a negative constant, so long as the local angle of attack remains below the local stalling angle. If the wing angle of attack at the center line, $\alpha_w(0)$, is large, then the incremental value due to p may take some sections of the wing beyond the stalling angle. When this happens $|C_{l_p}\hat{p}|$ is reduced in magnitude

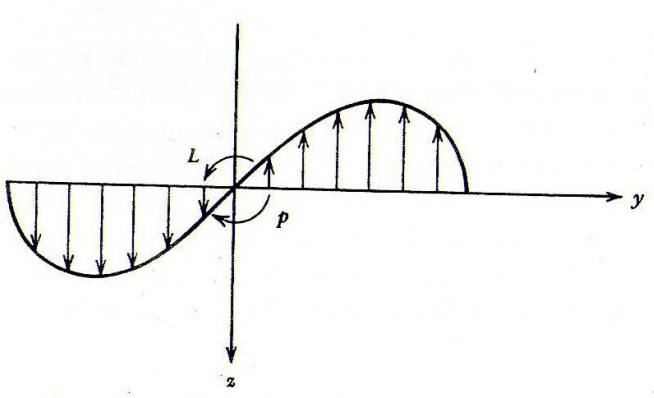

FIGURE 3.2: Spanwise lift distribution due to rolling.[20]

from the linear value and if $\alpha_w(0)$ is large enough it will even change sign. When this happens, the wing will autorotate: the main characteristic of spinning flight.

Roll control is, usually, achieved by the differential deflection of ailerons or spoilers, δ_a, which modify the spanwise lift distribution creating the roll moment around the longitudinal axis. From the literature[21] one knows that a simple strip integration can be obtained to estimate the roll control effectiveness of an aileron. In the present case, the lack of ailerons or spoilers in the wing lead us to a new approach: roll control power must be estimated in terms of span extension rather than aileron deflection. Therefore, the designation $C_{l_{\delta_a}}$ no longer makes sense, being the new derivative designated by C_{l_y}. Both C_{l_p} and C_{l_y} are obtained in the next section with all the assumptions made.

3.2 Mathematical Model

In order to calculate the available roll moment, l, at each flight speed, some considerations must be made. Firstly, the lift distribution along the wing is supposed to have a perfect elliptical form. Secondly, no fuselage data is considered, so that only the wing is taken into account. Therefore, no losses are considered, like downwash effect and fuselage interferences. The following analysis for the VSW was performed taking into account winspan length variation for each flight speed.

Consider an ellipse whose center is allowed to move along the y-axis. From the caracteristic expression of the ellipse (see Figure 3.3) one has:

$$z = a\sqrt{1 - \left(\frac{2y}{b}\right)^2} \tag{3.1}$$

The corresponding correction for the ellipse position is given by:

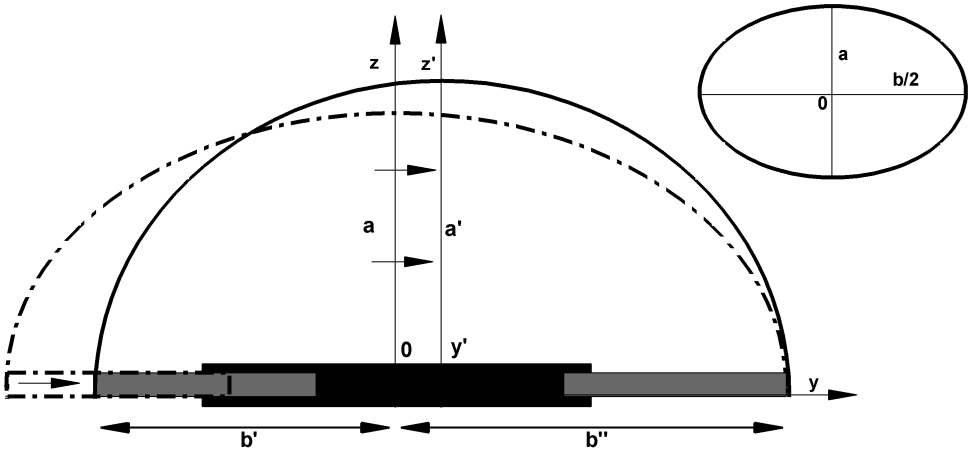

FIGURE 3.3: Change in neutral roll point due to asymmetric variations in span.

$$z' = a'\sqrt{1 - \left(\frac{2(y - y')}{b}\right)^2} \tag{3.2}$$

where $b = b' + b''$.

Aerodynamically one knows that the rolling moment due to the lift distribution along the wingspan is:

$$l = \frac{1}{2}\rho V^2 \int_{-b'}^{b''} C_l(y)c(y)ydy \tag{3.3}$$

As exemplified with the generic ellipse correction in Equation 3.2, the corrected lift distribution is given by:

$$C_l(y)c(y) = a'\sqrt{1 - \left(\frac{2(y - y')}{b}\right)^2} \tag{3.4}$$

Since a' is not known, an approximation has to be made. Considering that the semi-ellipse area is equal to $C_L S$, one can state that:

$$\frac{\pi a' b}{2 \times 2} = C_L S \tag{3.5}$$

From the definition of C_L:

$$C_L = \frac{2W}{\rho V^2 S} \tag{3.6}$$

and substituting for $C_L S$ in Equation 3.5 one has, for a':

$$a' = \frac{8W}{\pi b \rho V^2} \tag{3.7}$$

From this result, the expression for C_{l_y}, after dividing Equation 3.3 by $1/2\rho V^2 S_{ref} b_{ref}$, is given by:

$$C_{l_y} = \frac{8W}{\pi b \rho V^2 S_{ref} b_{ref}} \int_{-b'}^{b''} y \sqrt{1 - \left(\frac{2(y-y')}{b}\right)^2} dy \tag{3.8}$$

Considering now that the aircraft is in a steady turn with an angular velocity p, the roll moment generated around the fuselage longitudinal axis is l. The increment in angle of attack from the root to the tip of the wings is given by:

$$\Delta\alpha = \frac{py}{V} \tag{3.9}$$

Because $C_l(y) = a_{0_y}(y)\Delta\alpha$, one can say that:

$$C_l = \frac{1}{S_{ref} b_{ref}} \int_{-b'}^{b''} a_{0_y} \frac{py}{V} c(y) y dy \tag{3.10}$$

As in the C_{l_y} calculation, the lift slope $a_{0_y}(y)$ needs a small correction due to the change in lift distribution. For a given old $a_0(y)$ coordinate, the lift slope value will now correspond to $a_0(y + \Delta y)$. The lift slope $a_0(y)$ is given by the aerodynamic optimization tool. Then, the correction factor becomes:

$$a_{0_y}(y) = a_0(y) \sqrt{1 - \left(\frac{(y-y')}{b/2}\right)^2} \tag{3.11}$$

Therefore,

$$C_{l_p} = -\frac{1}{V S_{ref} b_{ref}} \int_{-b'}^{b''} a_0(y) \sqrt{1 - \left(\frac{(y-y')}{b/2}\right)^2} c(y) y^2 dy \tag{3.12}$$

The roll rate for the morphing wing can be calculated by:

$$p = \frac{C_{l_y}}{C_{l_p}} \tag{3.13}$$

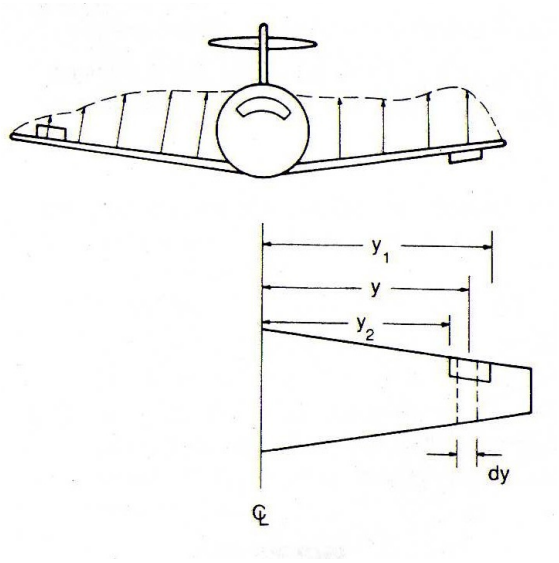

FIGURE 3.4: Strip theory approximation of roll control effectiveness.[21]

In order to make a roll performance comparison between the new telescopic wing and the original fixed wing, one must estimate the roll rate exhibited by the ailerons that it is fitted with. From reference[21] we know that the control power $C_{l_{\delta_a}}$ can be obtained by:

$$C_{l_{\delta_a}} = \frac{2C_{L_{\delta_a}}}{S_{ref}b_{ref}} \int_{y_1}^{y_2} c(y)ydy \tag{3.14}$$

where

$$C_{L_{\delta_a}} = \frac{\partial C_L}{\partial \delta_a}\delta_a \tag{3.15}$$

and

$$\frac{\partial C_L}{\partial \delta_a} = \frac{\partial C_L}{\partial \delta_f} \tag{3.16}$$

and y_1 and y_2 are defined in Figure 3.4.

From reference[22] one has:

$$\frac{\partial C_L}{\partial \delta_f} = 0.9K_f \left(\frac{\partial C_l}{\partial \delta_f}\right)_{airfoil} \frac{S_{flapped}}{S_{ref}} \cos\lambda_{H.L.} \tag{3.17}$$

where the theoretical lift increment for plain flaps, $\frac{\partial C_l}{\partial \delta_f}$, is about 3.7 (per degree) for the original SG 6042 with an aileron with 20% chord ratio, and K_f, an empirical correction for plain flaps, is about 0.9. H.L. refers to the flap hinge-line sweep and $S_{flapped}$ refers to the portion of the wing with the flap.

Similarly to the *damping-in-roll* derivative for the telescopic wing but without the lift distribution correction, C_{l_p} for the original wing is given by:

$$C_{l_{p_{aileron}}} = -\frac{1}{VS_{ref}b_{ref}} \int_{-b/2}^{b/2} a_0(y) \sqrt{1 - \left(\frac{2y}{b}\right)^2} c(y) y^2 dy \tag{3.18}$$

Finally, the roll rate for the original wing can be calculated by:

$$p = \frac{C_{l_{\delta_a}}}{C_{l_{p_{aileron}}}} \delta_a \tag{3.19}$$

The full span integration includes three main wing parts: the central fixed wing, and the two movable tip wings. Span variation was made with increments of 10% for both left and right tip wings. All the combinations, symmetric and asymmetric, were performed. The flight speed range used was that of the aerodynamic analysis, from 10.75 to 50 m/s. In the original fixed wing analysis, the flap deflection was performed from 0 to 20 degrees.

3.3 Roll Rate Results

The trends illustrated in Figure 3.5 to 3.10 are the results for the static stability analysis. The calculations were conducted in the range of speed already described. Span variation on both tip wings include all symmetric and asymmetric cases. The lift distribution correction was performed taking into account the three main wing parts, the central fixed wing, and the two movable ones.

The *damping-in-roll* coefficient results show that roll damping increases as wingspan increases, which is in agreement with other works.[15, 16] These results are a consequence of the conservation of angular momentum.[16] Increasing the span decreases p, the rate of roll, whereas decreasing the span tends to speed up the roll rate. One can observe too that C_{l_p} in the morphing wing is inversely proportional to the flight speed. This was expected from expression 3.11, since C_{l_p} is inversely dependent on V. Roll rate in the original wing, considering roll control by aileron deflection, shows a linear growth as deflection increases. One can see that the VSW matches the aileron performance in

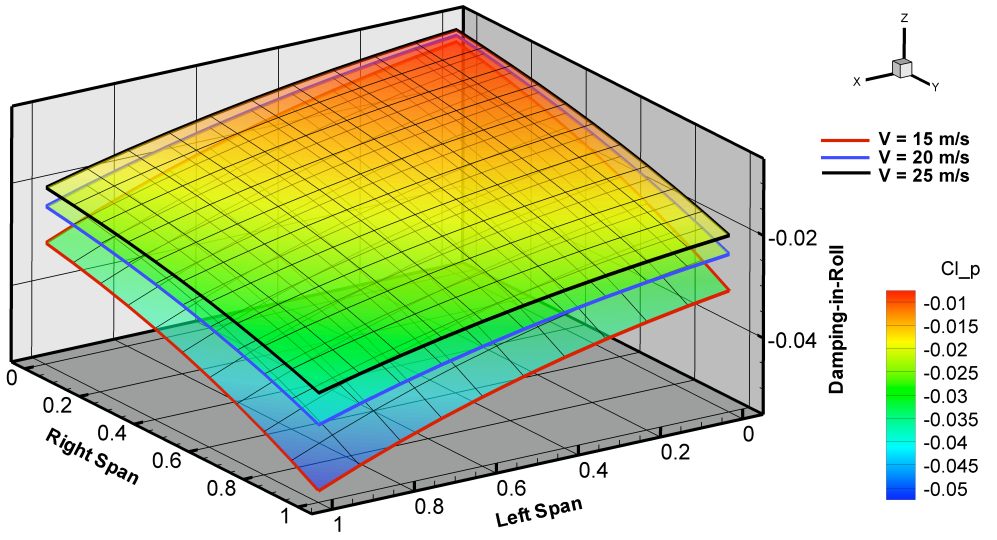

FIGURE 3.5: Damping-in-roll moment coefficient for asymmetric wing variations at 15, 20 and 25 m/s flight speed.

terms of roll power. The roll rate achieved increases as flight speed increases, being the maximum roll rate values similar to those achieved by the VSW. One can conclude that the rolling control is possible with asymmetric span variations, and that VSW is capable of performing steady turns.

Roll power, C_{l_y}, grows with the increase in wingspan differential. The increase in speed reduces the tendency of the aircraft to roll, as the damping increases, which is very consistent with the C_{lp} results. One can observe that roll rate for the VSW decreases with the increase in speed, contrary to what happens in a wing with ailerons.

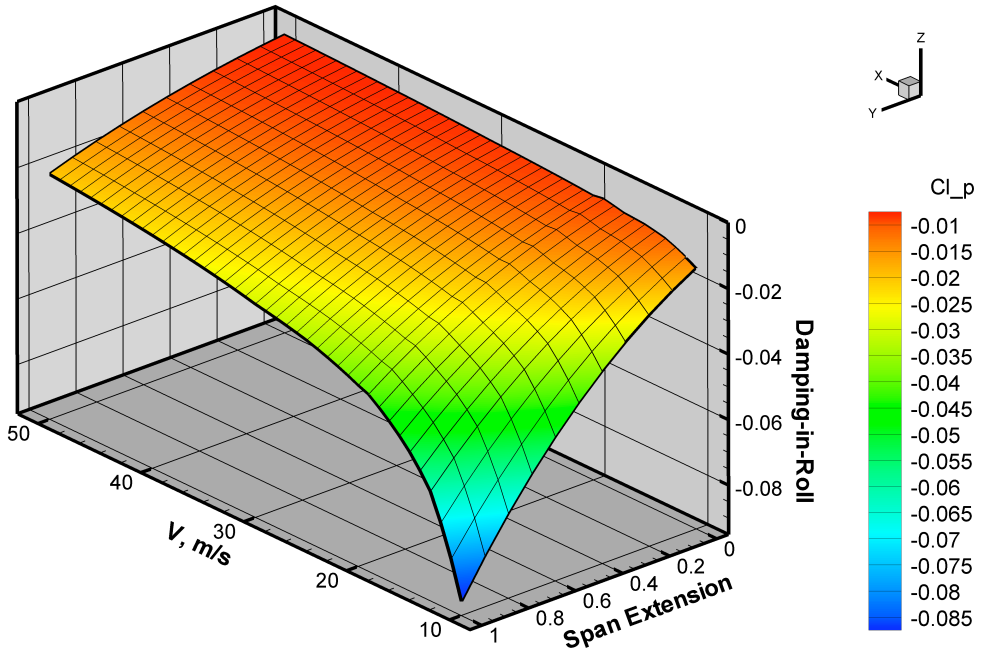

FIGURE 3.6: Damping-in-roll moment coefficient for symmetric wing variations.

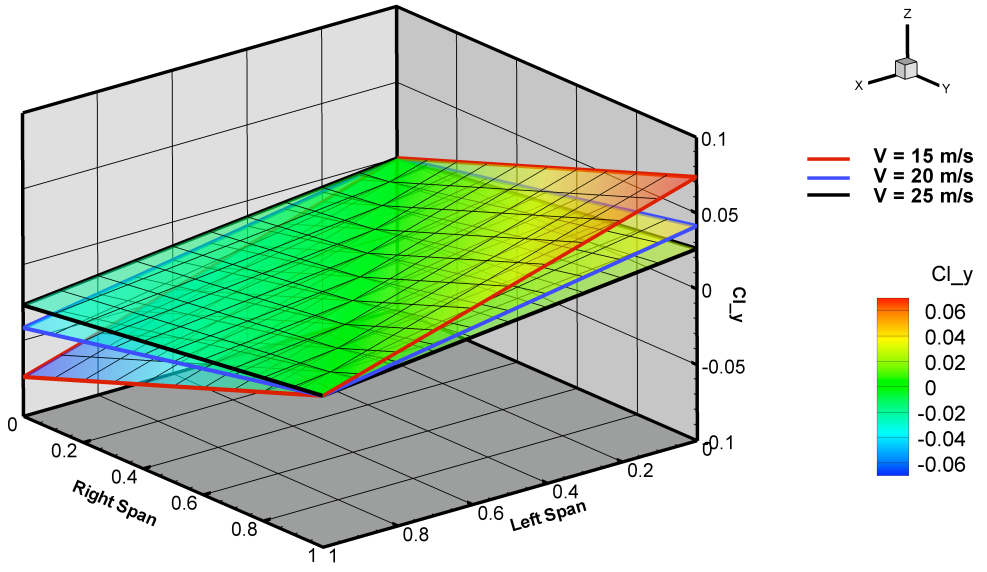

FIGURE 3.7: Roll power for VSW.

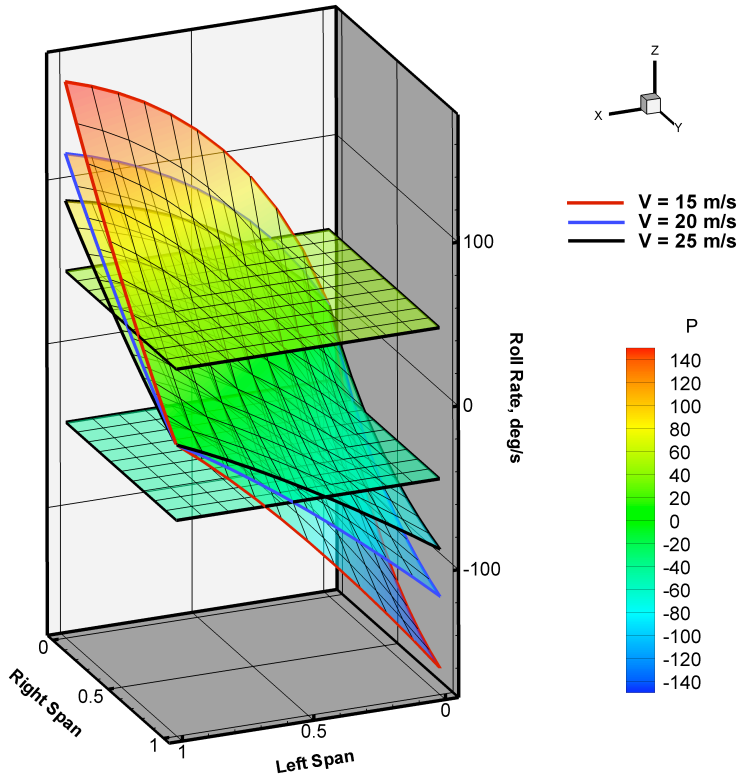

FIGURE 3.8: Roll rate variation for a flight speed of 15, 20 and 25 m/s.

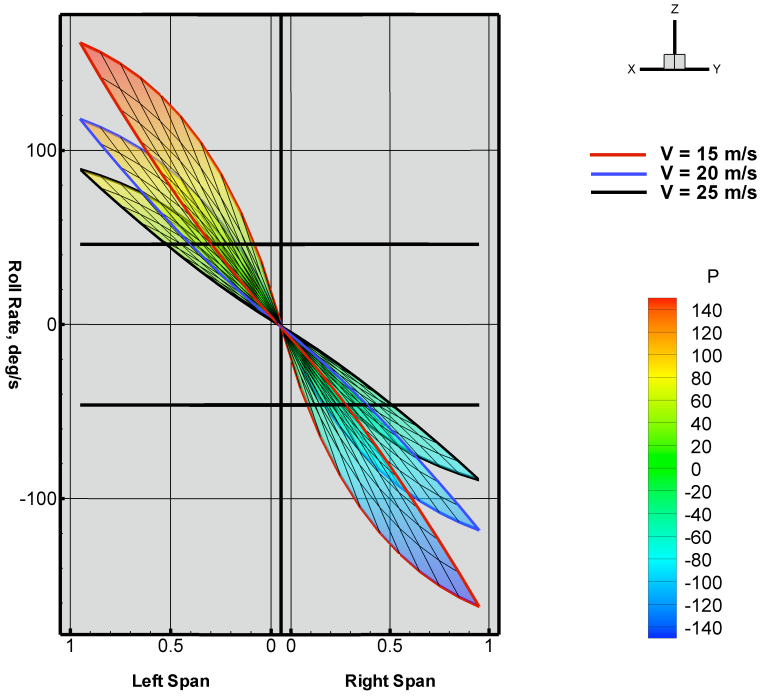

FIGURE 3.9: Results of the roll rate for the VSW.

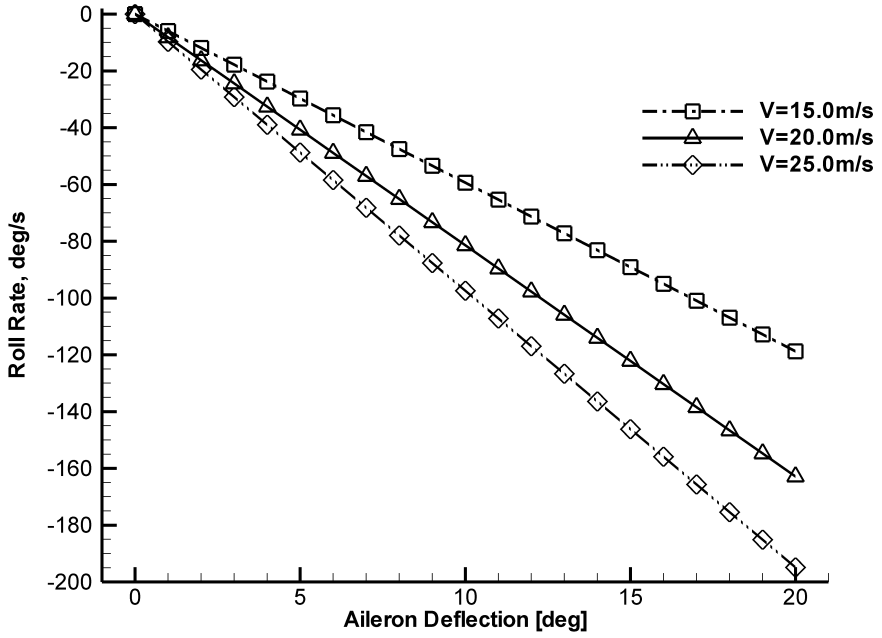

FIGURE 3.10: Roll rate available for the original wing with ailerons at 15, 20 and 25 m/s.

Chapter 4

System Design and Construction

4.1 Wing Design

4.1.1 Outer Moving Wing

The variable-span morphing concept in the present work includes a fixed bigger, hollow wing (IFW), and a small outer wing that is movable (OMW). The design used in the movable wings is very conventional: the wings are composed of ten 2 mm thick balsawood ribs, a 195g/m^2 carbon fiber/epoxy skin and a carbon circular tube spar. As referred in Chapter 2, the maximum span length was set to be the same as the original fixed wing: 2.5 m. This fact implicated a pre-sizing of the complete wing set. In order to have a 2.5 m total span length, it was estimated that both inner and outer wing parts would have a 0.625 m length, and based on the experience acquired in UAV construction, that 0.1 m of minimum wing overlapping would allow a sufficient wing stiffness in the full extended configuration. Figure 4.1 shows the wing configuration and Table 4.1 the wing final dimensions taking into account Equations 4.1. Knowing that b_{max} is 2.5 m and that the fuselage width, L_{fus}, is 0.2 m one can estimate the IFW and OMW length, X and Y, respectively. The distance between the OMW ribs, d_{ribs}, was set to 0.07 m. The required rack stroke, S_{rack}, and length, L_{rack}, were estimated taking into account that the rack will be attached to the first two ribs of the OMW to reinforce the assembly. R is simply a length increment to ensure that, on a fully deployed situation, the rack maintains the contact with the actuator pinion. The overall system was drawn and studied in a CAD/CAM tool.

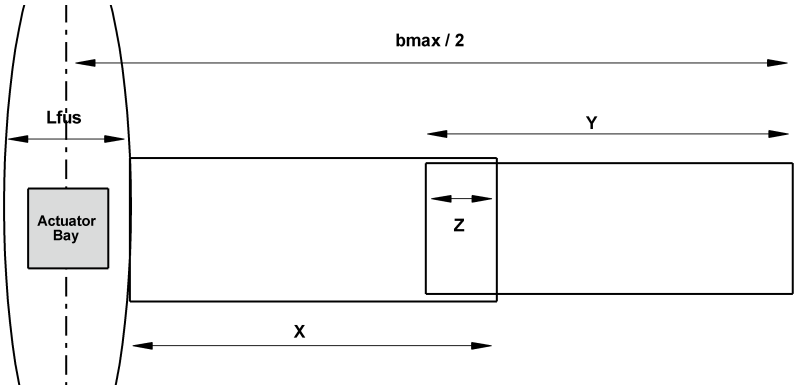

FIGURE 4.1: Pre-dimensioning variables of the VSW.

$$\begin{aligned} \frac{b_{max}}{4} &= X = Y \\ S_{rack} &= X - Z \\ L_{rack} &= S_{rack} + \frac{L_{fus}}{2} + d_{ribs} + R \end{aligned} \tag{4.1}$$

The OMW negative mould was made from glass fiber to obtain the correct skin shape. In order to guarantee perfect shaping of the leading-edge, the upper and lower surfaces were not separated at the chord line. Instead, the upper surface part of the mould was extended from the leading-edge to the lower surface. Figure 4.2 illustrates the concept. This negative mould was obtained from a positive mould, constructed in foam and covered by glass fiber. The main spar on the OMW is circular, an unconventional approach in the sense that, despite ensuring a good resistance to bending, it is also used to align the OMW with the IFW. The spar is a carbon fiber tube with 1mm thickness and an outer diameter of 20 mm. The alignment between wings is assured with another carbon fiber tube, with a smaller outer diameter: 18 mm. This smaller tube fits in the larger tube perfectly in order to prevent any slack. Because the IFW had to be hollow, the smaller inner tube is not connected to it. Instead, it is in a floating condition, just fixed to the root rib and fuselage. Both tubes were sized in order to assure sufficient bending stiffness. From reference[23] one knows that the bending stress on a beam is given by:

$$\sigma = \frac{M}{I} c \tag{4.2}$$

where M is the bending moment at the section, I is the second moment of area of the cross-section and c is the distance from the neutral axis to the outermost fiber of a symmetrical beam section.

For a tubular beam, with a circular cross-section (see Figure 4.3), one has:

Variable	b_{max}	L_{fus}	X	Y	Z	S_{rack}	L_{rack}	d_{ribs}	R
Dimension, m	2.500	0.200	0.625	0.625	0.100	0.525	0.755	0.070	0.060

TABLE 4.1: Wing dimensions obtained from expressions 4.1.

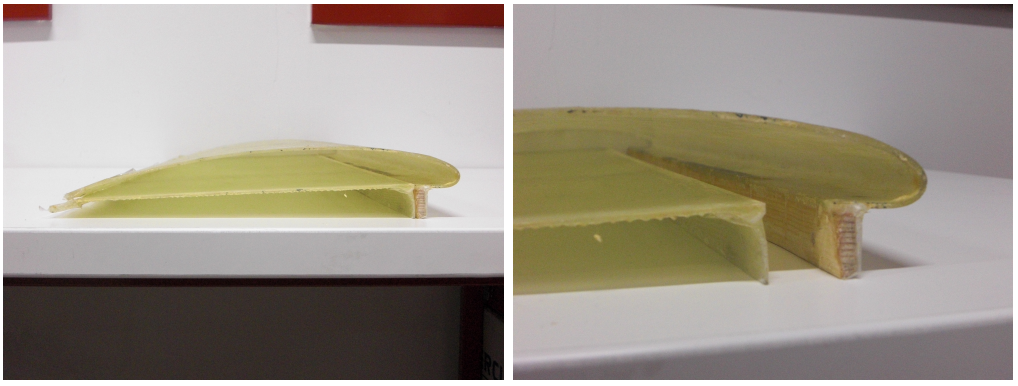

FIGURE 4.2: OMW glass fiber negative mould: the complete set (left); leading-edge detail (right).

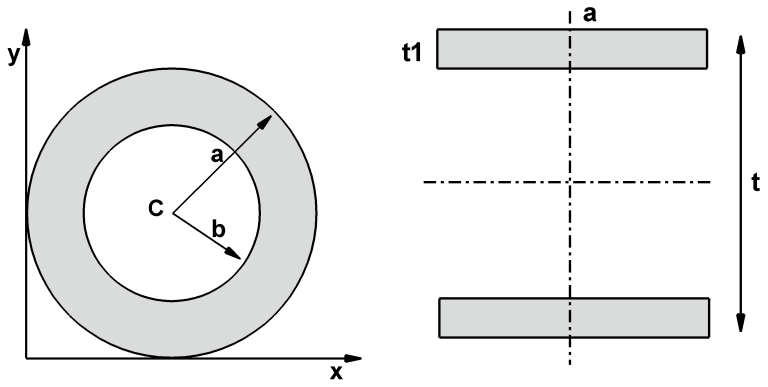

FIGURE 4.3: Spar cross-section: circular on the inner wing (left); rectangular on the outer wing (right).

$$I_{xc} = I_{yc} = \frac{\pi(a^4 - b^4)}{4} \tag{4.3}$$

The ribs were perforated in order to attach both the circular spar and a rack-guide tube. The rack beam used to push/pull the wing is made of balsawood and has a 4 mm×4 mm cross-section with a glued reinforced plastic rack removed from an ordinary printer. It is 0.755 m long, which is more than enough to span the wing length of 0.625 m and the stroke needed of 0.525 m. For example, it crosses the left tip wing when the right tip wing is in a fully contracted position. To prevent the wing rack from getting stuck when crossing the ribs, a rack-guide tube was made from epoxy impregnated glass fiber tube. This glass fiber tube was glue-assembled at the ribs just like the circular spar. This rack system has proven to be enough to actuate the tip wing and although the rack exhibits

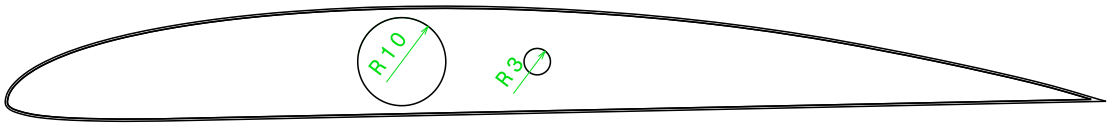

FIGURE 4.4: Rib sketch with the perforations to assemble both circular spar and rack-guide tube in the OMW.

some bending, it is not enough to impaire its smooth motion. The OMW assembly was performed in the following sequence:

i) After using a negative mould to laminate the carbon fiber skin; the skin was cut in the correct dimensions;

ii) The ribs were cut in the right dimensions and perforated to assemble both the circular spar and the rack-guide tube;

iii) The 20 mm outer diameter carbon tube was cut (0.625 m) and attached to the ribs using epoxy glue;

iv) The rack-guide glass fiber tube was attached to the ribs using epoxy glue as well;

v) The rack was attached to the two first ribs;

vi) The wing was covered with the carbon skin, which was attached to the ribs with epoxy glue.

4.1.2 Inner Fixed Wing

The IFW design differs from the OMW design. The need to have a hollow wing, in order to allow the OMW to slide inside it, requires a different design approach. In the OMW, the main circular spar conferred the sufficient bending stiffness while the ribs provided the correct wing shape. In the IFW the skin is required to both provide the correct shape and resist the bending moment resulting from the wing extension. This was achieved with an unusual main spar configuration (see Figure 4.5) and reinforcing the skin with two layers of carbon fiber forming spar caps. The spar was sized according to reference[23] using Equation 4.2 to estimate bending stresses in beams. Because the two beams are rectangular (see Figure 4.3), one has, for the second moment of area of the spar,

$$I_x = 2\left[\frac{at_1^3}{12} + at_1\left(\frac{t - t_1}{2}\right)\right] \tag{4.4}$$

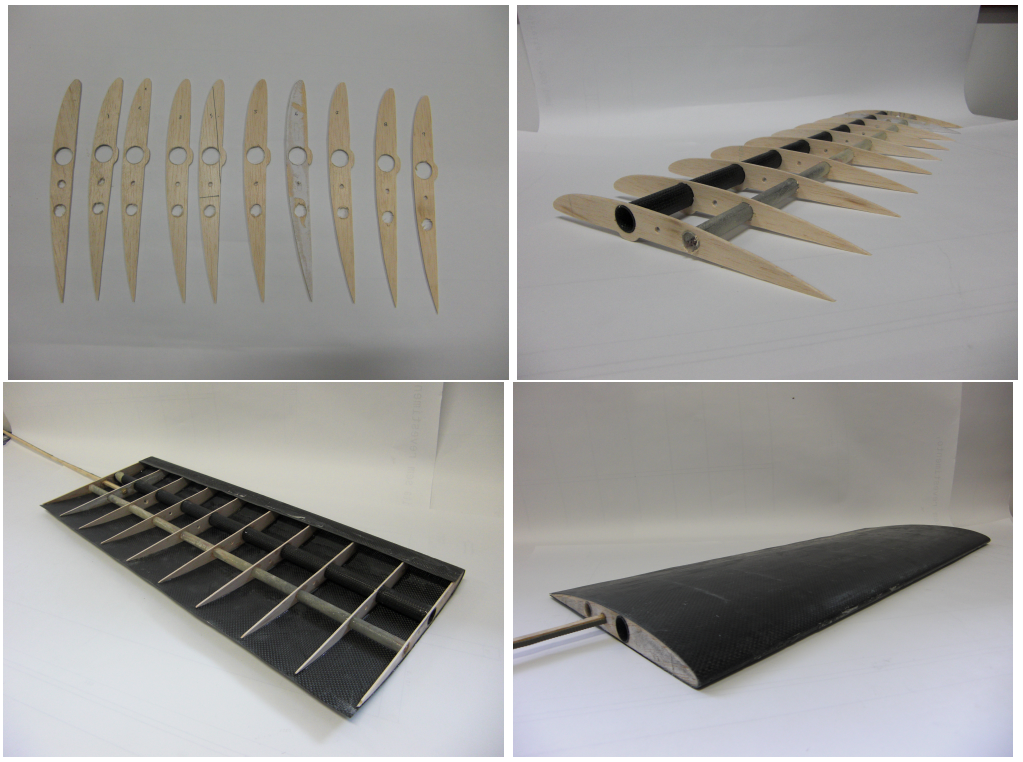

FIGURE 4.5: OMW during assembly process.

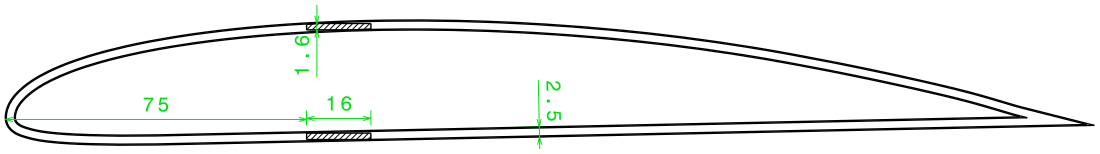

FIGURE 4.6: Main spar configuration and position on the IFW.

According to Figure 4.3, the final dimensions of both IFW and OMW spars are presented in Table 4.2.

The IFW was made using the positive mould used to obtain the OMW negative mould. This allowed a construction from inside out guaranteeing the most small space between wings, to avoid slacks. From inside out, the load carrying skin was achieved with a layer of 90 g/m^2 carbon fiber, a layer of 2 mm porous PVC foam and another layer of 90 g/m^2 carbon fiber. PVC foam was incorporated between the carbon fiber layers to allow the incorporation of the main spar and to give adequate stiffness to the skin since there are no ribs present. The complete assembled skin has a 2.5 mm thickness, which originated a fairly acceptable small discontinuity between wing seams in the full span condition. Because this was a major problem observed in some works[2, 3, 4] this issue was treated with great care.

In a posterior phase it was decided to prolong the rectangular spar set to attach the two

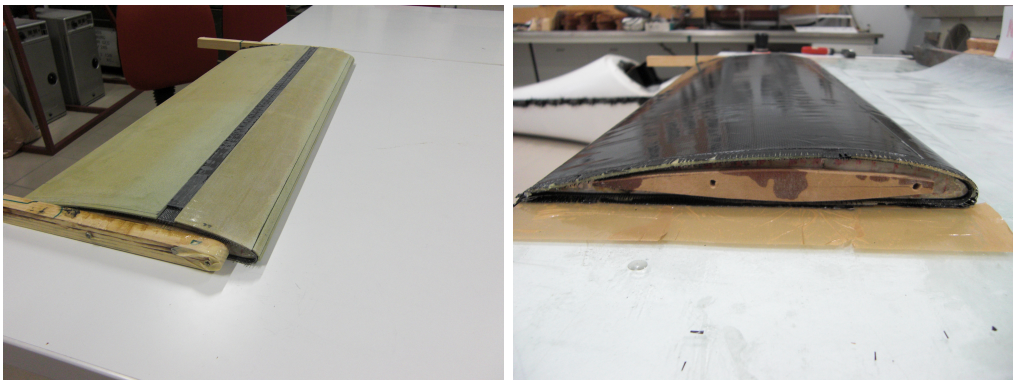

FIGURE 4.7: IFW construction: with the first and second layers of carbon fiber and porous PVC foam, respectively (left); with the final carbon fiber layer (right).

IFW	OMW
a=16 mm	a=10 mm
t1=1.6 mm	b=9 mm
t=30.5 mm	

TABLE 4.2: Final dimensions for OMW and IFW spars.

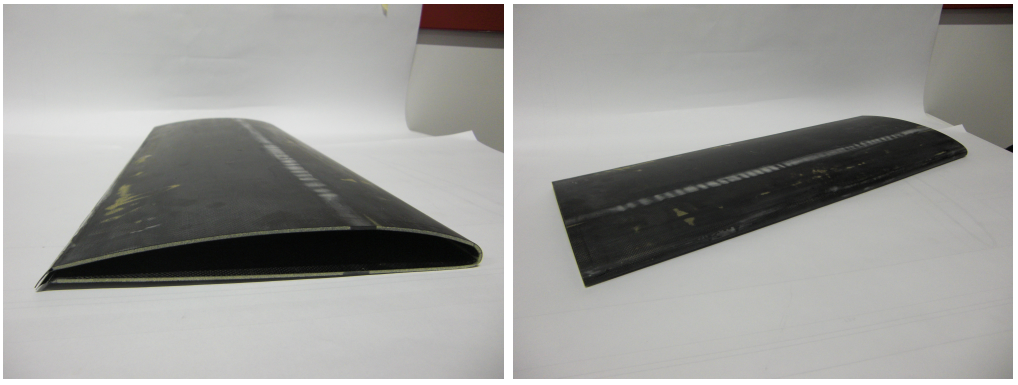

FIGURE 4.8: IFW final aspect.

support elements (that fix the wing system to the fuselage) in order to ease the bending in the inner carbon fiber tube.

4.2 Actuation Mechanism

4.2.1 Actuator Requirements

The aim of the VSW project was not a one-time full deployment and no contraction system. Instead, the system was required to allow in-flight expansions and contractions of the wing, in order to perform a full-time wing aspect ratio adaptation to the flight

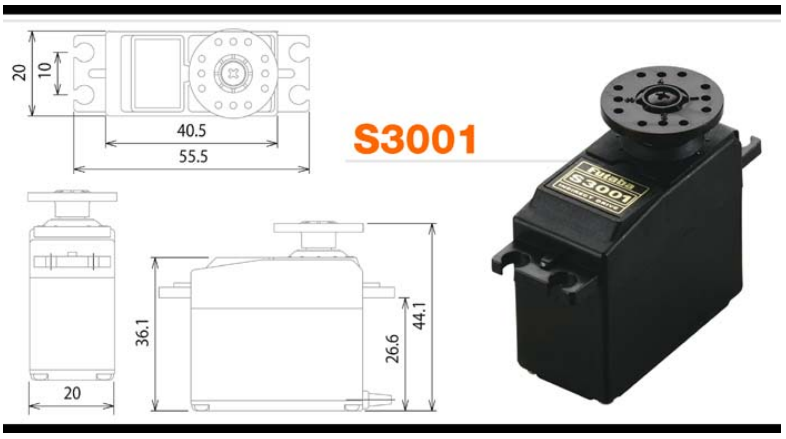

FIGURE 4.9: Standard S3001 Futaba servo chosed for wing actuation.[24]

regimes. Deployable inflatable wings were, at the very beginning, excluded. An electro-mechanical system was chosen as the most plausible way to achieve what was proposed. Several actuation mechanisms were pondered: servo, electric step-motor and brushless ordinary electric motor. The choice from the three kinds of mechanism was largely dependent on the way it was intended to actuate the wing. A leading-screw mechanism actuation system was considered; so a fast rotation electric brushless motor appeared as the best choice, since not much torque was needed to perform the back and forth movement. However, a leading-screw system tends to become very heavy because of the required screw length (in our case 525mm) and large energy losses due to friction between elements occurs. Therefore, a simple rack and pinion system was best suited for the purpose: lighter and fast enough if actuated properly. Either a servo or a step-motor were suited for a rack and pinion system, which needs more torque and control precision than the leading-screw mechanism. The final decision was influenced by wing control issues. The step-motor has good torque and quick response but is not prepared to be radio-controlled as a servo is. RC servos are composed of an electric motor mechanically linked to a potentiometer. Pulse-width modulation (PWM) signals sent to the servo are translated into position commands by electronics inside the servo. When the servo is commanded to rotate, the motor is powered until the potentiometer reaches the value corresponding to the commanded position. This feature allows a servo to be positioned just by modulating the frequency in the radio controller. In future work, a possible development of an automatic span extension controller should be facilitated by this choice. So, more than its known affordability and reliability, was the control simplicity that led to the choice of a servo-mechanism as a mean to actuate the wing.

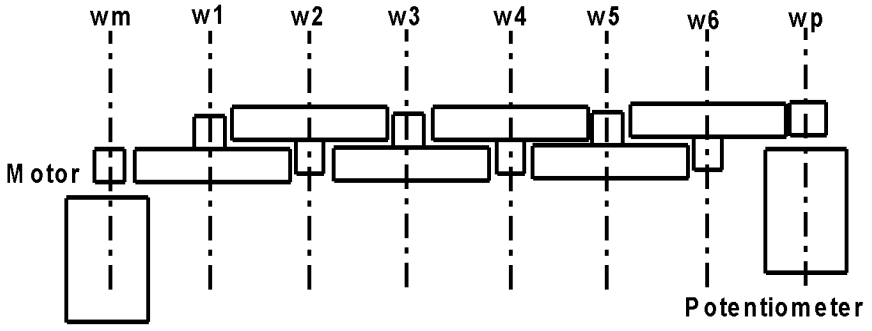

FIGURE 4.10: Representative diagram of the reduction gears system used in the actuation mechanism.

Set	m-1	1-2	2-3	3-4	4-5	5-6	6-p
Reduction	0.163	0.219	0.299	0.444	0.219	0.299	0.444

TABLE 4.3: Obtained reduction of each set of gears.

4.2.2 Sizing and Assembling

As mentioned, the motor of a RC servo is mechanically linked (via reduction gears) to a position feedback potentiometer. Although, this reduction is considerably small in terms of linear length covered by the movement transmitter pinion (about 63 mm in the case of the S3001 Standard Futaba[24] servo). This limitation is imposed by the potentiometer angular motion, which is almost 2/3 of a turn, more exactly 210 degrees. In order to perform the required 525 mm wing stroke length for 2/3 of a turn in the potentiometer, it was necessary to add more reduction stages. This was achieved by adding the reduction stages of a second S3001 Futaba servo to the first one. One can easily find the necessary reduction by the reduction ratio of each gear set and angular velocity at the motor (see Table 4.3). Figure 4.10 presents a simple diagram of the reduction gear system. Being w_m, w_i and w_p the angular velocity at the motor, at each i gear set, and at the potentiometer, respectively.

The necessary reduction was given by:

$$w_p = 0.04 w_2 \tag{4.5}$$

The original S3001 Futaba servo has the transmission pinion at the w_1 stage of the reduction gear system, so a new shaft was made in order to couple the pinion on the second gear stage. Figure 4.11 shows the final assembled servo-mechanism. The new servo was benchtested and it was proved that, with a full charged battery supply, it can perform a full 0.525 m deployment in 2.3 seconds, which is quite good for required span deployment quickness. A torque estimation was also performed and it was found that

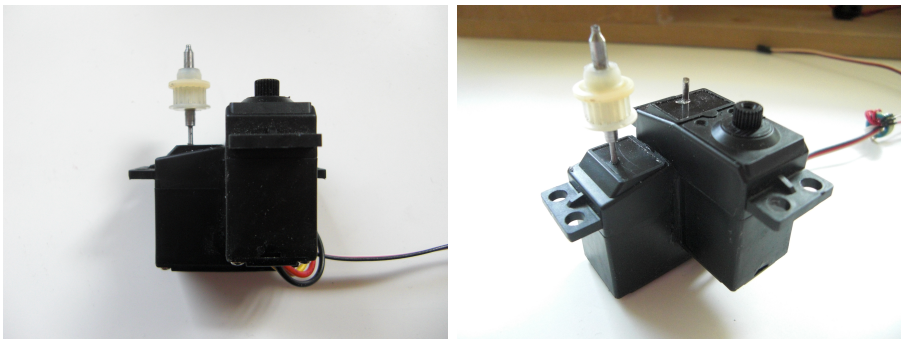

FIGURE 4.11: Assembled new servo-mechanism.

the given modified servo-mechanism exhibited a 0.300 Nm torque, which means it can push/pull a 680 g mass. The estimation of the OMW mass is under 300 g, so it was considered enough to actuate the wing.

4.2.3 Actuator Bay

The actuator bay is one of the most important elements of the complete wing/actuator system. The bay was specially designed to carry the servo-actuators and maintain them in the correct position when the wing is deployed. Its shape and design was dictated by the space that the new fuselage could provide (see Figure 4.12) and also by the need to maintain construction simplicity and functionality. It incorporates the holes to couple the servo-mechanisms as well as a small spring positioned between the rack and the actuator pinion, and is made of 2 mm thick plywood. The spring maintains a small pressure on the rack so that it is kept always against the pinion in order to prevent the rack to slip or jump on the pinion in situations that require more torque to move the OMW; and it is simply composed of two thin strips of steel forced by two supports. After being built, the concept revealed itself a bit stiffer than desired, with too much friction between the spring and the rack. This fact led to a modification in the concept for bench testing. The initial concept was replaced by the rotating attenuator used in the earlier servo-mechanism tests. Both concepts are presented in Figure 4.13.

Two small supporting elements were made to allow the attachment of both wings and the actuator bay. These elements were built from 5 mm plywood and two 7 mm outer diameter aluminum tubes to attach the wings to the fuselage.

The concept of the whole bay is clearly seen in Figure 4.14. The complete bay is attached to the wing, becoming a one system together with the wing.

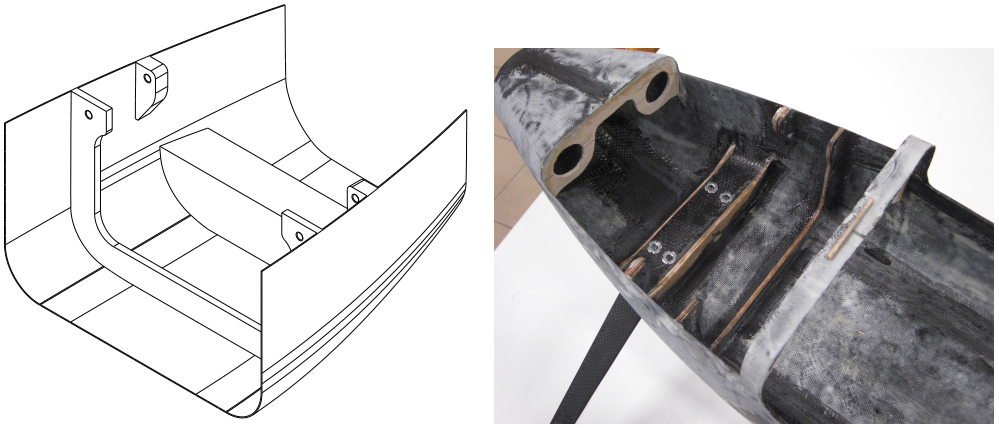

FIGURE 4.12: New fuselage bay area: in CAD/CAM sketch (left); in the real fuselage (right).

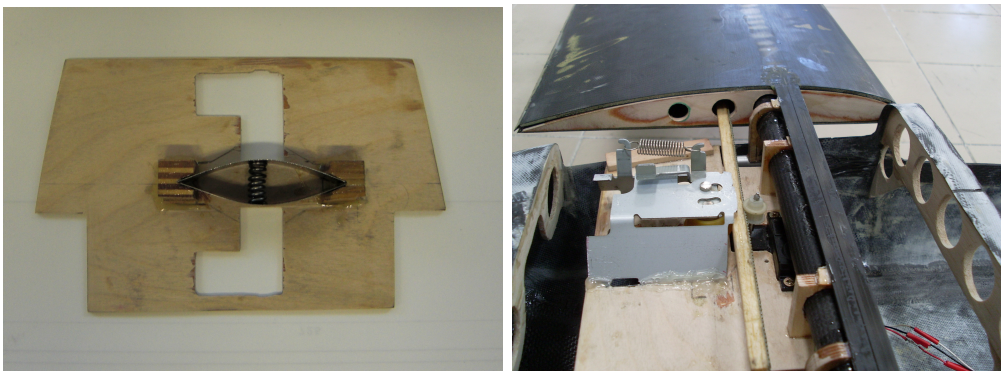

FIGURE 4.13: Actuator bay: original attenuator mounted on the actuator bay (left); attenuator used for bench testing (right).

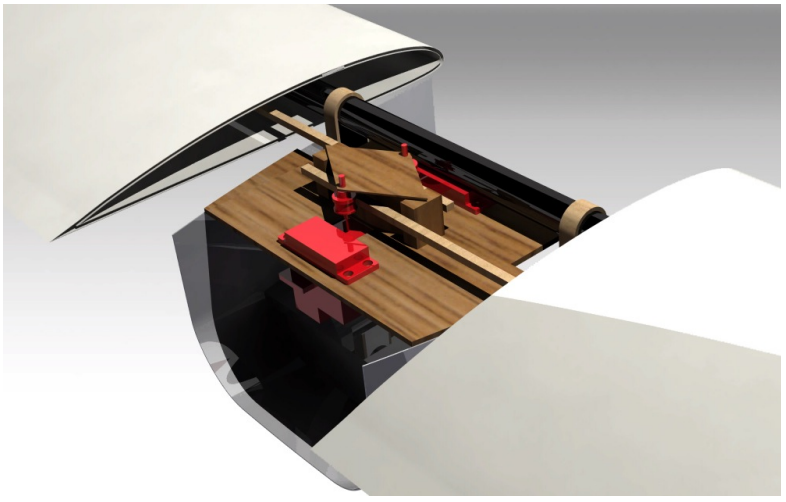

FIGURE 4.14: Rendered image of the original actuator bay and IFW from CAD/CAM design.

Chapter 5

Wing Testing

5.1 Final Assembly

The final assembly was achieved following the steps below:

i) The IFW was cut in the correct dimensions;

ii) The servos were mounted in the actuator bay along with the spring;

iii) The two support elements were fixed to the fuselage;

iv) The actuator bay was mounted in the correct position in the new fuselage bay area;

v) The inner carbon fiber tube was mounted in the two support elements, and attached at the same time to the actuator bay;

vi) The IFW plywood rib was assembled in the inner carbon fiber tube and then attached to the root of the IFW;

vii) The rectangular main spar set of the IFW was extended to attach the two support elements;

viii) The OMW was assembled inside the IFW and the rack was inserted in the pinion.

All parts were weighted during the assembly process. Table 5.1 shows each element mass and the overall system estimated and measured mass.

The original pair of wings that equip UAV Olharapo has a mass of 1065 g, but adding the original flight control system of servos and cables (70 g) and the new wing union part to attach in the new fuselage (135 g) the sum of the parts becomes 1270 g. So, the original

Part	Qty.	Element	Mass [g]
OMW	20×	2mm balsawood ribs	28
	2×	Carbon fiber tube	88
	2×	Actuator rack	12
	2×	Glass fiber tube	38
	2×	Carbon fiber skin	328
IFW	2×	IFW	685
	4×	Rectangular spar extension	39
	2×	Plywood rib	26
Actuator bay	2×	Modified servo-mechanism	103
	1×	Actuator bay (with spring)	60
	2×	Support elements	14
		Estimated overall mass	1421
		Measured overall mass	1547
		Mass of epoxy-resin	126

TABLE 5.1: Mass of each element of the VSW system.

overall wing system has only 277 g less than the VSW system, which is 57.4% less than the 650 g increment on the aircraft's weight assumed in the aerodynamic optimization input. This 57.4% mass margin can be used to reinforce the wing structure in order to reduce the deformations observed and to apply a wing position control system that depends on the flight speed and the load factor.

It was found during the assembly process that the wing set created a negative dihedral angle due to the weight of the wing when fully deployed. A considerable torsion on both IFW and OMW was also noted. This fact was accentuated by the fact that the fuselage, because it is in an early phase of construction, does not have a proper reinforced area to attach to the wing. Therefore, it was decided that the bench testing should not be performed with the wing attached to the real fuselage. This could result, especially in the wing load test, in severe damage to the fuselage and wing. So, a wood support was made to attach the wing for bench testing.

FIGURE 5.1: Assembled VSW on UAV Olharapo's new fuselage.

5.2 Bench Testing

The bench testing aimed at evaluating the real performance of the overall system. Two simple tests were to be performed: (a) an extension/retraction of the wing without wing loading, measuring the deployment time; and (b) a structural test by simulating a 6G wing load, approximately 18 kg in the present case for only one wing.

The deployment test revealed that the servo adopted was unable to accomplish with ease the extension/retraction cycle of the wing, making impossible the measurement of the deployment time. Therefore, the torque necessary to move the wing was checked. It was found that one needs a force of 6.521 N to move the wing, corresponding to a torque of 0.294 Nm (despite the OMW having only 2.422 N, the friction force between wing elements increases the force needed to move the wing in about 270%). Since the servo maximum available torque is 0.300 Nm, one can easily conclude that it is working near its limit. Further work must be done in order to minimize the resulting friction drag between the OMW and the IFW elements. One can also conclude that the servo used is not powerful enough to actuate the wing. Even if friction between elements is greatly reduced, one has to take into account the extra friction that will arise from the in-flight wing load distribution. Small building errors resulted in geometry differences from design: negative dihedral and twist. These significantly affect the correct deployment of the wing and are the major causes to the high friction forces encountered.

The wing load test was performed with sand bags (see Figure 5.2) - twelve 1 kg bags + six 0.5 kg bags + twelve 0.25 kg bags - approximating the load distribution to a constant distribution on the IFW and a triangular distribution on the OMW. The load was distributed over the wings' main spars to avoid torsion, and was carried out progressively from 1G to 6G. The results were not as good as expected, since the wing load only reached 3.5G (10 kg) revealing a large torsion on both wings. Further work must be done also at structural level, since the trailing-edge must be well attached to the fuselage

FIGURE 5.2: Sandbags used for wing load testing.

FIGURE 5.3: VSW load test: with no load (top left); with 1G - 3 kg (top right); with 2G - 6 kg (bottom left); with 3.5G - 10 kg (bottom right).

to avoid torsion as in the original wing design. Despite the torsion observed, both the IFW and the OMW revealed good resistance to bending. Figure 5.3 shows the wing load test process.

Chapter 6

Summary

6.1 Conclusions

The present work led to major conclusions about the functioning of variable-span morphing wings.

The aerodynamic analysis revealed that, at low speeds, the original wing has better performance than the VSW. This can be explained by the performance reduction of the modified SG6042 used in the VSW, and because of the higher relative thickness ratio of the IFW airfoil. The IFW presents a slightly higher drag value at low speeds when the wing is fully extended. This led to a slight increase in the stall speed, which was 11 m/s in the original wing, and became 11.25 m/s in the VSW. On the other hand, this performance tendency is inverted beyond 22.5 m/s, when the VSW outperforms the original wing. At 25, 30 and 40 m/s one registered 5.08%, 18.28% and 32.93% drag reduction with the VSW. This is due to the reduction of the wing area and consequently the total drag relatively to the original wing.

The rolling rate analysis conducted shows that the roll damping on the VSW increases as the wingspan increases which is a consequence of the conservation of angular momentum. Increasing the span decreases the roll rate, which is in good agreement with previous works. C_{l_p} is inversely proportional to the flight speed as well, i.e., contrary to what happens with ailerons, the roll damping increases as flight speed increases. Therefore, for a given wingspan the VSW becomes more stable with the increase in flight speed. One observed also that the roll power, C_{l_y}, exhibited by the VSW matches the aileron performance, being the maximum roll rate values similar in both cases for a given speed. Therefore, one can conclude that the VSW is capable of performing steady turns with asymmetric span control, without the need of ailerons.

Both deployment and wing load tests revealed some major problems on the VSW. It was found that the friction force between the elements of the IFW and the OMW and the actuation system led to an increase of 270% in the force necessary to move the wing. So, the available torque of 0.300 Nm revealed insufficient to easily move the OMW, which requires a torque of 0.294 Nm. The small difference between the required and the available torque led to mediocre actuation performance. The wing load test revealed excessive negative wing dihedral and torsion as already noted when the VSW was assembled. This, is believed, was due to small construction errors. Both effects are considered the main causes for such high friction force between wing elements. The VSW reached 3.5G (10 kg) of wing load and, despite the excessive torsion registered, the VSW concept revealed good resistance to bending and an acceptable overall performance. Future work in the system must seek better adapted solutions: a stronger servo for the actuation system and, during the construction process, a great diligence and accuracy when making the several components of the system to avoid every kind of small errors that can negatively influence the performance of the system.

6.2 Future Work

Improvements are possible in almost any engineering design. In the present work, some areas for future work can be identified.

The modification of the original SG 6042 lower surface, which was implemented to simplify the construction of the wing prototype led to some performance losses, especially noted at lower speeds. Future improvements will require the use of the original airfoils in both inner and outer wing elements; perhaps using different airfoils on the two wing elements: a high speed airfoil for the IFW and a low speed airfoil in the OMW, in order to enhance overall wing performance for the complete speed range.

A more exhaustive aerodynamic analysis can also be performed using, along with the optimization code, a CFD study in order to identify any geometry detail that can be improved to enhance the aerodynamic performance of the wing.

One has seen that the VSW is very demanding at structural level. Therefore, a finite element model (FEM) can be developed to better size the wing structure to avoid excessive bending and torsion while keeping the weight low.

Since only half-wing was built, it is important that the construction process is continued so that a complete prototype is prepared for in-flight tests. Some modifications and refinements must be implemented to avoid some of the errors incurred during the construction and assembly process.

One can conclude that the actuating system must be improved as well. A rack and pinion system is good but it requires a servo-mechanism with enough power to perform what is required. Other concepts must be addressed as well, like a leading-screw mechanism with a fast step motor for quick deployment and built in light materials.

Control issues are of paramount importance in morphing technologies. The need to operate simultaneously more and more complex structures, modify and adapt them to all flight conditions and do it in useful time is a real and demanding problem. The solution relies not on the pilot, not on the human brain, but in the machine. To continue developing this work a span controller is needed to ensure a correct wing deployment at each flight condition. The retraction and extension of the wings must be performed automatically. This requires knowledge of flight speed and normal acceleration through sensors. A quick look at the roll control issue shows at least three possible situations to be considered to perform a steady turn from an initial cruise condition: at low speeds, with the wings fully deployed, one has to retract the inside-turn wing; at medium speeds, with the wings half deployed, one must retract the inside-turn wing and extend the outside-turn wing (this can be performed proportionally or not); and at high speeds, with the wings fully retracted, one has to extend the outside-turn wing. Also, it is important to quantify the energy requirements to actuate this wing during a full typical mission and compare those with the original conventional wing with ailerons. By doing this it will be possible to assess whether the performance advantages of the variable span wing are not offset by power and weight requirements.

Bibliography

[1] S. Joshi, Z. Tidwell, W. Crossley, and S. Ramakrishnan. Comparison of morphing wing strategies based upon aircraft performance impacts. *AIAA Paper 2004-1722*, April 2004.

[3] J. Blondeau and D. Pines. Design and testing of a pneumatic telescopic wing for unmanned aerial vehicles. *Journal of Aircraft*, 44(4):1088–1099, July-August 2007.

[8] D. Cadogan, W. Graham, and T. Smith. Inflatable and rigidizable wings for unmanned aerial vehicles. *AIAA Paper 2003-6630*, Sepember 2003.

[10] D. Cadogan, S. Scarborough, D. Gleeson, A. Dixit, J. Jacob, and A. Simpson. Recent development and test of inflatable wings. *AIAA Paper 2006-2139*, May 2006.

[17] J. Bae, T. Seigler, D. Inman, and I. Lee. Aerodynamic and static aeroelastic considerations of a variable-span morphing wing. *AIAA Paper 2004-1726*, April 2004.

[19] D. Neal, M. Good, C. Johnston, H. Robertshaw, W. Mason, and D. Inman. Design and wind-tunnel analysis of a fully adaptive aircraft configuration. *AIAA Paper 2004-1727*, April 2004.

[5] J. Vale, P. Gamboa, F. Lau, and A. Suleman. Optimization of a morphing wing based on coupled aerodynamic and structural constraints. *3rd AIAA Multidisciplinary Design and Optimization Specialist Conference*, Honolulu, Hawaii, USA, April 2007.

[20] B. Etkin and L. Reid. *Dynamics of Flight: Stability and Control.* John Wiley and Sons, Inc., third edition, pp. 150-151. 1996.

[21] R. Nelson. *Flight Stability and Automatic Control.* McGraw-Hill Book Company, international edition, pp. 75-77, 107-108. 1990.

[24] Hobbico Inc. Futaba s3001 servo, June 2009. URL `http://www.futaba-rc.com/servos/servos.html`.

[2] J. Blondeau, J. Richeson, and D. Pines. Design, development and testing of a morphing aspect ratio wing using an inflatable telescopic spar. *AIAA Paper 2003-1718*, April 2003.

[4] J. Blondeau and D. Pines. Pneumatic morphing aspect ratio wing. *AIAA Paper 2004-1808*, April 2004.

[6] P. Gamboa, P. Aleixo, J. Vale, F. Lau, and A. Suleman. Design and testing of a morphing wing for an experimental uav. *The Applied Vehicle Technology Panel Symposium (AVT-146)*, Florence, Italy, May 2007.

[7] M. Czajkowski, G. Clausen, and B. Sarh. Telescopic wing of an advanced flying automobile. *AIAA Paper 975602*, 1997.

[9] D. Cadogan, T. Smith, F. Uhelsky, and M. MacKusick. Morphing inflatable wing development for compact package unmanned aerial vehicles. *AIAA Paper 2004-1807*, 2004.

[11] J. Jacob, S. Smith, R. Jones, S. Scarborough, and D. Cadogan. A high-altitude test of inflatable wings for low-density flight applications. *AIAA Paper 2006-1696*, May 2006.

[12] S. Scarborough, J. Rowe, S. Smith, A. Simpson, and J. Jacob. Development of a finite element model of warping inflatable wings. *AIAA Paper 2006-1697*, 2006.

[13] J. Jacob, S. Smith, D. Cadogan, and S. Scarborough. Expanding the small uav design space with inflatable wings. *07ATC-217, Society of Automotive Engineers Inc.*, 2007.

[14] L. Kheong and J. Jacob. In flight aspect ratio morphing using inflatable wings. *AIAA Paper 2008-425*, January 2008.

[15] J. Henry, J. Blondeau, and D. Pines. Stability analysis for uavs with a variable aspect ratio wing. *AIAA Paper 2005-2044*, April 2005.

[16] J. Henry and D. Pines. A mathematical model for roll dynamics by use of a morphing-span wing. *AIAA Paper 2007-1708*, April 2007.

[18] J. Bae, T. Seigler, and D. Inman. Aerodynamic and static aeroelastic characteristics of a variable-span morphing wing. *Journal of Aircraft*, 42(2):528–534, March-April 2005.

[22] D. Raymer. *Aircraft Design: A Conceptual Approach*. Education Series. American Institute of Aeronautics and Astronautics, Inc., fourth edition, pp. 477. 2006.

[23] *Fundamentals of Engineering Supplied-Reference Handbook*. National Council of Examiners for Engineering and Surveying, fifth edition, pp. 29, 30, 32. 2001.

[25] E. Stanewsky. Aerodynamic benefits of adaptive wing technology. *Aerosp. Sci. Technol. 4 (2000) 439-452*, S120-9638(00)01069-5/FLA, 2000.

[26] L. Iannucci and A. Fontanazza. Design of morphing wing structures. In *3rd SEAS DTC Technical Conference*, Edinburgh, 2008.